

Characterizing temporally resolved connectivity patterns in transient brain states with lifespan aging

Mrittika Dey

*A Dissertation submitted to the
National Brain Research Center
for the award of
Masters in Neuroscience
(2020-2022)*



National Brain Research Centre
(Deemed to be University)
Manesar, Haryana, India - 122052

द्रीय मस्तिष्क अनुसंधान केंद्र (समविश्वविद्यालय)



(जैव एवं प्रौद्योगिकी विभाग का स्वायत् संस्था,
विज्ञान एवं तकनीकी मंत्रालय, भारत सरकार)
न० एच०-०८, मानेसर-१२२ ०५२ (हरियाणा), भारत

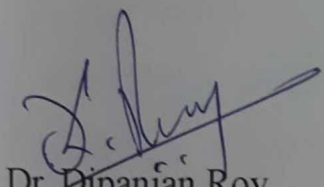
National Brain Research Centre (Deemed University)

(An Autonomous Institute of Deptt. of Biotechnology,
Ministry of Science & Technology, Govt. of India)
NH-08, Manesar - 122 052 (Haryana), INDIA

CERTIFICATE

This is to certify that the ^{dissertation report} *D.R. 07/06/22* thesis entitled “Characterizing temporally resolved connectivity patterns in transient brain states with lifespan aging” is the result of work carried out by **Mrittika Dey** in National Brain Research Centre, Manesar, Haryana, India.

The work presented herein is original and has not been submitted previously for the award of any degree or diploma to **National Brain Research Centre (Deemed to be University)** or to any other University. The work is as per the guidelines given by **National Brain Research Centre** and is a record of the candidate's own efforts.



Dr. Dipanjan Roy
(Supervisor)

Prof. Pravat K. Mandal
(Director, NBRC)

Place : Manesar
Date: 8th June, 2022

DECLARATION BY CANDIDATE

I, Mrittika Dey, hereby declare that the work presented in the dissertation report entitled "**Characterizing temporally resolved connectivity patterns in transient brain states with lifespan aging**" was carried out by me under the guidance of Dr. Dipanjan Roy, Scientist IV & Associate Professor, Division of Computational Neuroscience, **National Brain Research Centre (Deemed to be University)**, Manesar, Haryana, India.

I declare that no part of the thesis contains any plagiarised material. Any previously published or other material sourced from anywhere else has been appropriately attributed to the source. I also declare that no part of this thesis has been previously submitted for the award of any degree of diploma to **National Brain Research Centre (Deemed to be University)** or to any other university.


Mrittika Dey

Place : Manesar

(Name and Signature of the candidate)

Date : 8th June, 2022

Acknowledgement

First and foremost, I would like to acknowledge and express my deepest sense of gratitude to my supervisor, Dr Dipanjan Roy, without whom the completion of this study would not be possible. His expertise, guidance and advice not only helped me steer the project in the right direction but also augmented my knowledge in the fascinating world of neuroscience.

I extend my gratitude to all my lab members who taught me the importance of a great work ethic and were always open to discussing ideas, which has inspired me greatly. I am really indebted to Nisha Shastry, for the patience and time she imparted in helping me understand the nuances of the HMM model, and for her constant support and faith.

I am really thankful to Alish Dipani, for teaching me how to be a better scientist and for always having my back. I am grateful to my friends, Madhumita, Rimil and Vinayak as well as my batchmates and seniors for being my family away from home.

Lastly, I would like to thank my family for always supporting me, believing in me, and giving me the strength to pursue my passion.

Mrittika Dey

Contents

Acknowledgement	iv
Lists of Figures	xii
Lists of Tables	xiv
Abstract	xv
1 Introduction	1
1.1 Neurobiological basis of age-associated decline in cognitive abilities	3
1.2 Functional basis of age-associated decline in cognitive abilities	4
1.2.1 Oscillatory activity, Coherence and Power	4
1.2.2 Network Connectivity	5
1.3 Spontaneous brain activity	7
1.3.1 Hidden Markov Model	8
1.3.2 HMM in transient brain dynamics	10
1.4 Scope of dissertation	12

2 Materials and methods	14
2.1 MEG Analysis	14
2.1.1 Participants	14
2.1.2 Data Acquisition	14
2.1.3 Source Reconstruction	15
2.2 Data for hidden Markov modeling	15
2.2.1 Preprocessing	15
2.2.2 Source reconstructed dipole ambiguity	16
2.2.3 Time-delay embedded Hidden Markov Model	16
2.2.4 Similarity between inferences	17
2.2.5 Age-wise group HMM estimation given state course probabilities	17
2.3 Resting State Temporal Dynamics	18
2.3.1 Transition Probabilities	18
2.3.2 Fractional Occupancy	18
2.3.3 Dwell Times	18
2.3.4 State switching rates	19
2.4 Spectral Statistics	19
2.4.1 Spatial activation maps	19
2.4.2 Non-parametric estimation of state spectra	19
2.4.3 Change in global coherence and phase coupling	20
2.4.4 Connectivity analysis	20
2.4.5 Statistical Analysis	21

3 Results	22
3.1 The activation pattern of states follows a distinct trend with age	22
3.2 Temporal Dynamics	28
3.2.1 The probability of transitioning between states remain stable with age	28
3.2.2 Fractional Occupancy of states in all age groups	29
3.2.3 The mean lifetime of a state's activation	31
3.2.4 State switching rates	33
3.3 Spectral Dynamics	34
3.3.1 Change in state specific global coherence with frequency	34
3.3.2 Global coherence in theta and alpha bands show inverse age-related trends	40
3.4 Network Connectivity	46
3.4.1 Phase based connectivity in the brain does not show dynamic changes with age	46
3.4.2 Connectivity analysis in specific parcels of power activation	49
4 Discussion	61
5 Conclusion	66
References	68
Appendix	75

List of Figures

1.1	Large scale networks identified by performing independent component analysis on fMRI data. Source: Heine et al., 2014	6
1.2	An example of Markov chain. Source: kdnuggets.com (Markov chains) .	9
1.3	Example of Hidden Markov Model. Source: vitalflux.com (Data Analytics)	10
1.4	General schematic of the analysis pipeline used in employing time delay embedded HMM to source reconstructed MEG data.	12
3.1	Mean activation in each age group: States are arranged in ascending order of mean functional activation in each age group. The red line signifies the mean activation in each state over all brain regions, the black line signifies the median.	23
3.2	Statewise parcel activation compared across age groups: Comparison of the mean activation value in activated clusters or regions in each state across all four age groups. The red line inside each box signifies the mean.	25
3.3	Volumetric maps showing spatial activation pattern: Functional connectivity maps showing the spatial activation pattern in all eight states across age groups. Red color signifies higher functional connectivity in those regions compared to the global average.	26

3.4	Surface maps showing spatial activation pattern: Functional connectivity maps showing the spatial activation pattern in all eight states across age groups. Functional connectivity in the regions higher than the global average show warmer colors (red). Regions showing lower activation than global average are marked with cooler colors (blue).	27
3.5	Transition probability across all age groups	29
3.6	Fractional Occupancy of each state across all age groups	30
3.7	Fractional Occupancy correlation: Correlation matrix between the fractional occupancy time courses of each state for a) Young, b) Early Middle, c) Late Middle, d) Old age groups. Positive correlations between states indicate that the two states are visited together more frequently during similar timepoints.	31
3.8	Mean lifetimes of the states in each age group. The black line inside each violin denotes the mean of the distribution. The median is indicated by a red line. A higher mean lifetime indicates fewer fluctuations and more stability of a particular state.	32
3.9	Mean state switching rate in all age groups	33
3.10	Spectral Profile: Data driven decomposition of the spectra in all age groups resulted in the division of a) wideband (0-40 Hz) spectra into three different frequency modes. The peak frequency (modes) obtained in the spectral profiles resembles the classical b) theta (0.5-10 Hz), c) alpha (5-15 Hz) and d) beta (15-30 Hz) ranges in all age groups.	35
3.11	Global coherence in all states: Global coherence over all pairs of regions in the wideband frequency range, plotted in the increasing order of mean coherence for all age groups. Mean coherence for each state is marked in red.	36
3.12	Global coherence in all states in the theta frequency range: Global coherence over all pairs of regions in the theta band frequency range plotted in the increasing order of mean coherence for all age groups. Mean coherence for each state is marked in red.	37

3.13 Global coherence in all states in the alpha frequency range: Global coherence over all pairs of regions in the alpha band frequency range plotted in the increasing order of mean coherence for all age groups. Mean coherence for each state is marked in red.	38
3.14 Global coherence in all states in the beta frequency range: Global coherence over all pairs of regions in the beta band frequency range plotted in the increasing order of mean coherence for all age groups. Mean coherence for each state is marked in red.	40
3.15 Comparison of change in coherence in the wideband frequency range for each state across all age groups. The box plots show the mean and distribution of the global coherence in the wideband thresholded power spectra. Mean coherence for each age group is marked in red.	42
3.16 Comparison of change in coherence in the theta band (0.5-10 Hz) frequency range for each state across all age groups. The box plots show the mean and distribution of the global coherence in the theta band thresholded power spectra. Mean coherence for each age group is marked in red.	43
3.17 Comparison of change in coherence in the alpha band (5-15 Hz) frequency range for each state across all age groups. The box plots show the mean and distribution of the global coherence in the alpha band thresholded power spectra. Mean coherence for each age group is marked in red.	44
3.18 Comparison of change in coherence in the beta band (15-30 Hz) frequency range for each state across all age groups. The box plots show the mean and distribution of the global coherence in the beta band thresholded power spectra. Mean coherence for each age group is marked in red.	45
3.19 Phase lag index: Comparison of strength of phase coupling in each state in the theta frequency range along each age group. Mean phase lag index for each state is arranged in ascending order for all ages.	47

3.20 Phase lag index: Comparison of strength of phase coupling in each state in the alpha frequency range along each age group. Mean phase lag index for each state is arranged in ascending order for all ages.	48
3.21 Spectral connectivity: Comparing the 50% strongest connections across age in the a) theta and b) alpha frequency bands in State 1. The nodes indicate the lobes to which the parcels (frontal, limbic, temporal, parietal and occipital). From left to right, connectivity patterns are shown for: Young, Early Middle, Late Middle and Old age groups.	50
3.22 Spectral connectivity: Comparing the 50% strongest connections across age in the a) theta and b) alpha frequency bands in State 2. The nodes indicate the lobes to which the parcels (frontal, limbic, temporal, parietal and occipital). From left to right, connectivity patterns are shown for: Young, Early Middle, Late Middle and Old age groups.	52
3.23 Spectral connectivity: Comparing the 50% strongest connections across age in the a) theta and b) alpha frequency bands in State 3. The nodes indicate the lobes to which the parcels (frontal, limbic, temporal, parietal and occipital). From left to right, connectivity patterns are shown for: Young, Early Middle, Late Middle and Old age groups.	54
3.24 Spectral connectivity: Comparing the 50% strongest connections across age in the a) theta and b) alpha frequency bands in State 4. The nodes indicate the lobes to which the parcels (frontal, limbic, temporal, parietal and occipital). From left to right, connectivity patterns are shown for: Young, Early Middle, Late Middle and Old age groups.	55
3.25 Spectral connectivity: Comparing the 50% strongest connections across age in the a) theta and b) alpha frequency bands in State 5. The nodes indicate the lobes to which the parcels (frontal, limbic, temporal, parietal and occipital). From left to right, connectivity patterns are shown for: Young, Early Middle, Late Middle and Old age groups.	56

3.26 Spectral connectivity: Comparing the 50% strongest connections across age in the a) theta and b) alpha frequency bands in State 6. The nodes indicate the lobes to which the parcels (frontal, limbic, temporal, parietal and occipital). From left to right, connectivity patterns are shown for: Young, Early Middle, Late Middle and Old age groups.	57
3.27 Spectral connectivity: Comparing the 50% strongest connections across age in the a) theta and b) alpha frequency bands in State 7. The nodes indicate the lobes to which the parcels (frontal, limbic, temporal, parietal and occipital). From left to right, connectivity patterns are shown for: Young, Early Middle, Late Middle and Old age groups.	58
3.28 Spectral connectivity: Comparing the 50% strongest connections across age in the a) theta and b) alpha frequency bands in State 8. The nodes indicate the lobes to which the parcels (frontal, limbic, temporal, parietal and occipital). From left to right, connectivity patterns are shown for: Young, Early Middle, Late Middle and Old age groups.	59

List of Tables

5.1	Pairwise comparison of cluster based activation values between the age groups. Multiple comparison was performed using Post Hoc Tuley's test for pairwise T-test and controlled for family wise error rate. The asterisk (*) denotes that the differences between the means of the two groups are significant in the 95% interval of confidence. NS denotes the difference between means are not significant.	75
5.2	Pairwise comparison of whole brain activation values between all states. Multiple comparison was performed using Post Hoc Tukey's test for pairwise T-test and controlled for family wise error rate. The asterisk (*) denotes that the differences between the means of the two groups are significant in the 95% interval of confidence. NS denotes the difference between means are not significant. A p -value of zero indicates that the first four digits after the decimal point are zeros.	76
5.3	Comparisons between transition probabilities from one state to another. An asterisk denotes statistical significance at alpha = 0.05, and NS denotes that the difference between group means are not significant at the given confidence interval.	77
5.4	Pairwise comparison of whole brain phase lag index values of all age groups in the theta band frequency range. Multiple comparison was performed using Post Hoc Tukey's test for pairwise T-test and controlled for family wise error rate. The asterisk (*) denotes that the differences between the means of the two groups are significant in the 95% interval of confidence. NS denotes the difference between means are not significant.	78

5.5	Pairwise comparison of whole brain phase lag index values of all age groups in the alpha band frequency range. Multiple comparison was performed using Post Hoc Tukey's test for pairwise T-test and controlled for family wise error rate. The asterisk (*) denotes that the differences between the means of the two groups are significant in the 95% interval of confidence. NS denotes the difference between means are not significant.	78
5.6	Cluster based coherence values and their comparison between age groups. The significant differences are denoted by an asterisk. Non-significant differences are marked as NS.	79
5.7	Cluster based PLI values and their comparison between age groups. Tables 5.7a and 5.7b shows no significant changes across age groups (NS = non-significant) in both of the frequency ranges.	80

Abstract

Healthy aging is associated with several cognitive impairments, including declined attention, working memory, decision-making, and processing speed. Studying perceptual processes occurring on a very fast timescale in the context of spontaneous reorganization of underlying large scale brain networks can be challenging using traditional neuroimaging approaches. In this study, we investigated spontaneous brain dynamics to characterize the neural correlates of the changes in cognitive abilities with aging. We used resting-state MEG data from Cam-CAN and employed a data-driven, statistical Bayesian modeling approach to define transient brain activity recurring over time. We compared activation patterns, temporal features, spectral properties and connectivity patterns in four age groups, Young (18-34 years), Early Middle-aged (35-49 years), Late Middle-aged (50-64 years) and Old (65-88 years). The activation pattern in all age groups was found to differ, and the overall functional connectivity within networks showed variable trends with age. The temporal features of these transient states were relatively stable and were not affected by aging. Global coherence in specific band-limited power spectra also showed consistent age-related changes in all transient states. We found that global coherence in the theta and alpha ranges follows opposite patterns of decline with age. The inverse relationship in these two dominant frequency bands suggests a compensatory mechanism in the brain that could help prevent functional cognitive decline. We also investigated the role of frequency in the connectivity dynamics and its alteration with age. Further, we were interested in understanding the contribution of phase coupling or synchronization in driving these connectivity changes. We found a more significant contribution of power and coherence over phase. Finally, the pattern of connectivity in the older age groups also suggested a compensation hypothesis, based on which the large scale networks might undergo reorganization and adapt to the detrimental effects of aging. The within-network connection strengths show variable selectivity for anterior vs posterior connections in both frequency bands.

Coherence based connectivity between significant clusters in the alpha range was more selective for posterior connections, while in the theta band, the anterior connections survived age-associated decline. In summary, our study investigated the temporal, spectral and activation properties of transient brain networks and explored the effect of lifespan aging on them, which has profound implications for age-related decline in functional cognition.

Chapter 1

Introduction

The neurobiology of healthy and pathological aging consists of cumulative lifespan associated alterations in multiple domains, including cell biology, protein chemistry, morphology, physiology, oscillatory activity, and behavior. Neural oscillations exist in a range of multiple frequency landscapes with associated timescales of cognitive processing. Considering the rapid aging of the world's population, it is crucial to understand the neural and functional correlates of the cognitive decline that is associated with healthy aging. The most noticeable changes in cognitive ability as a person grows older include a decline in performance on cognitive tasks requiring decision-making, speed of processing, working memory and executive cognitive function [1]. Some aspects of cognition, however, remain relatively stable across the lifespan. These include what is known as 'crystallized abilities', which are the acquired skills and memories over the lifespan. General knowledge, reading comprehension, retrieval of semantic knowledge (e.g. historical information, anecdotes), and vocabulary reflect the crystallized abilities that are relatively preserved as a person gets older.

With the increase in the number of older adults in the population, it is essential to understand how age impacts cognition and if preventative and treatment strategies can be developed to help preserve cognition with advancing age. This is also vital for an individual's functional independence and to conserve their quality of life. There are, however, certain limitations that arise when studying cognition in relation to aging [2]. Lifespan studies are often associated with recruitment or cohort biases. Cross-sectional studies comparing groups of subjects in specific age groups risk attributing the differences found between groups to age, while other unmeasured factors might be

ignored. Longitudinal studies, on the other hand, are susceptible to practice effects or survival bias [1, 3, 4]. The Cambridge Center for Aging and Neuroscience (Cam-CAN) project, launched in 2010, was a large-scale, collaborative, cross-sectional study at the University of Cambridge which aimed to overcome these challenges and confounds. The study used epidemiological, cognitive, and neuroimaging data from nearly 700 subjects between the ages of 18–88 to understand how individuals can best retain their cognitive abilities with advancing age.

In this study, we wanted to focus on how transient brain dynamics evolve with age. Communication between spatially distinct brain regions, even in the resting state, is known to be highly informative in predicting cognitive flexibility [5]. Information flow in the brain during rest is highly related to the embedded network topology, and the pattern of information transfer can facilitate higher cognitive functions. Previous studies have investigated resting-state connectivity across the lifespan using functional magnetic resonance imaging (fMRI) blood oxygen level-dependent (BOLD) signals from specific regions of interest (ROIs) [6, 7]. Whole-brain analysis has revealed several resting-state networks (RSNs) observed through changes in BOLD signals. These networks are highly resolved spatially, but due to the longer timescale of BOLD response (~ 10 seconds), the temporal resolution is limited to much slower timescales than the underlying neural processes. The ability of the brain networks to flexibly reorganize and coordinate over a millisecond timescale can be studied with magnetoencephalography (MEG) data [8], which provides excellent temporal as well as spatial resolution. It is relatively free of physiological noise [9] and is less sensitive to age-related changes in vascular factors [10]. We used resting-state MEG data from the Cam-CAN project, characterized transient network dynamics by employing a Hidden Markov Model on the source reconstructed data, and studied these transient states' temporal and spectral characteristics across the lifespan.

In the subsequent sections, we cover the literature review of studies on the age-related cognitive decline across multiple neuroimaging techniques, the rationale behind using a variational Bayes inference method like the Hidden Markov Model to study brain dynamics, followed by an overview of the scope of the dissertation.

Age and Cognition: A Literature Review

1.1 Neurobiological basis of age-associated decline in cognitive abilities

Dynamic changes in biological, physiological, environmental, and behavioral processes are associated with healthy aging. It is imperative to understand the anatomical and physiological alterations correlated with the decline in functional cognition. The key neurobiological mediators of age-related decline in cognitive abilities and the onset of such changes in the lifespan have been extensively studied using longitudinal as well as cross-sectional data sets and a range of techniques such as Magnetic Resonance Spectroscopy (MRS), Magnetic Resonance Imaging (MRI), Positron Emission Tomography (PET), Radiochemistry, and Diffusion Tensor Imaging (DTI). These studies have revealed that there is age-associated decline in whole-brain volume [11, 7, 12]. In a study by Kruggel et al., it was seen that the loss of gray matter volume was significantly higher than white matter volume with a highly significant increase in CSF volume [13]. These differences were mostly observed in anterior cingulate, orbitofrontal and lateral prefrontal cortices with little to no difference in volume in occipital and temporal lobes [12]. DTI studies have also shown that there is a significant decrease in white matter fractional anisotropy in healthy adults with age [14, 15] which suggests degradation of white matter microstructure. Interestingly, white matter degradation was seen to be selective to prefrontal regions of the brain but also encompassed frontocerebellar circuitry. Studies on quantitative changes in cortical thickness and shape of sulci and gyri with age revealed a pattern similar to a brain undergoing atrophy [16]. With increasing age, the cortical mantle was seen to become thinner, with most significant thinning seen in inferior prefrontal, precentral and supramarginal regions [17], with the gyri becoming narrower and more curved. The sulci, in turn, get broader and more flattened. In addition to these structural changes, some studies have also looked at the relationship between age-associated metabolic changes in the brain with cognitive functioning. Decrease in striatal dopamine binding [18, 19] and serotonin receptor binding in frontal and cingulate areas [20] have been found to be significant mediators in cognitive decline. These studies have provided an overall understanding of how the chemistry and morphology of major cognitive areas of the brain are affected as a person grows older.

1.2 Functional basis of age-associated decline in cognitive abilities

1.2.1 Oscillatory activity, Coherence and Power

Oscillatory activity in the brain is linked to a wide variety of perceptual, sensory, motor and cognitive operations. EEG studies have shown the correlation of periodic brain waves in particular frequency ranges with specific cognitive tasks.

For example, alpha (8-13 Hz) are the dominant oscillations in the brain that are traditionally believed to represent idling processes in the brain [21]. They are negatively correlated with cortical excitability and task performance but act as a major contributor to perceptual facilitation, spatial and selective attention [22], and feature-based visual attention [23]. There is a significant slowing of peak frequency, and decrease in power in the alpha band [24, 25] which has been reported to be a biomarker of healthy as well as pathological aging process [26, 27]. Additionally, Sahoo et al. found a linear decrease in the global alpha coherence with age [25].

Low-frequency theta (3-7 Hz) oscillations have also been studied in the context of development and aging. Both peak frequency and theta power were higher in older adults, with an associated non-linear increase in global coherence after the age of 50. Higher theta power may be interpreted to be indicative of slower cognitive speed and mild cognitive impairment. However, if the slowing of alpha frequency is taken into account, the increase in theta power associated with healthy aging might act as a compensatory mechanism to increase cognitive performance in tasks involving arithmetic, working memory, spatial navigation, and episodic memory encoding and retrieval [28, 29].

Beta band (14-30 Hz) activity is known to be reliably associated with movement planning, and execution [30, 31]. Prior to making a movement and during the movement itself, there is a strong decrease in beta activity which dissipates shortly after the movement concludes. This phenomenon, known as event-related desynchronization, is followed by a strong increase in power relative to baseline levels and is known as post-movement beta rebound. Studies have shown that these movement-related oscillatory patterns show a non-linear increase in power [32, 25, 31] and linear increase in spontaneous beta activity in the motor cortices [32]. Global coherence in the beta band has

not been seen to show any age-dependence [25].

1.2.2 Network Connectivity

Functional Connectivity (FC) is the measure of the strength of connection between two spatial distinct brain regions based on their co-activation over time. Two brain regions are considered ‘functionally connected’ when there is reliable covariation or correlation of their activities over time. Clustering algorithms, spatial independent component analysis (ICA), graph theory, and seed-based-based connectivity measures are usually applied to fMRI BOLD signals to characterize such synchronization. Even in the resting state (i.e. when a subject is not performing any tasks), studies have identified certain core, large-scale brain networks consisting of several discrete brain regions responsible for different cognitive functions. The major brain networks include the default mode network (DMN), salience network, dorsal attention network (DAN), executive control network, sensorimotor network, and the visual network (shown in Figure 1.1). fMRI studies have shown that functional connectivity in these large-scale brain networks gets reorganized as a consequence of widespread structural deterioration [33]

DMN is the most extensively studied network in the context of aging. Functional connectivity within the DMN has been found to decrease from early to late adulthood [34, 35]. Temporal correlation between the anterior and posterior part of DMN is found to be reduced in the case of older individuals [36, 37] which correlated with behavioral measures of decreased executive functioning and processing speed [34].

Studies on other functional networks, however, have had contrasting results. Some studies have found age-related decreases in functional connectivity in the visual network and increases in somatomotor, executive, frontoparietal and auditory networks [38]. Another study by Allen et al. (2011) [39], on the other hand, found a decrease in the majority of brain networks with age. Tomasi et al. (2011) [40] used a voxelwise, data-driven approach called functional connectivity density mapping (FCDM) to study age-related changes in short- and long-range FC measures in these networks. They found prominent decreases in short- and long-range FC measures in DMN and DAN and increases in somatosensory and cerebellar networks. For other networks, the decreases in long-range connectivity were, on average, more significant than short-range connectivity. Studies by Onoda et al. (2012) also found a decrease in

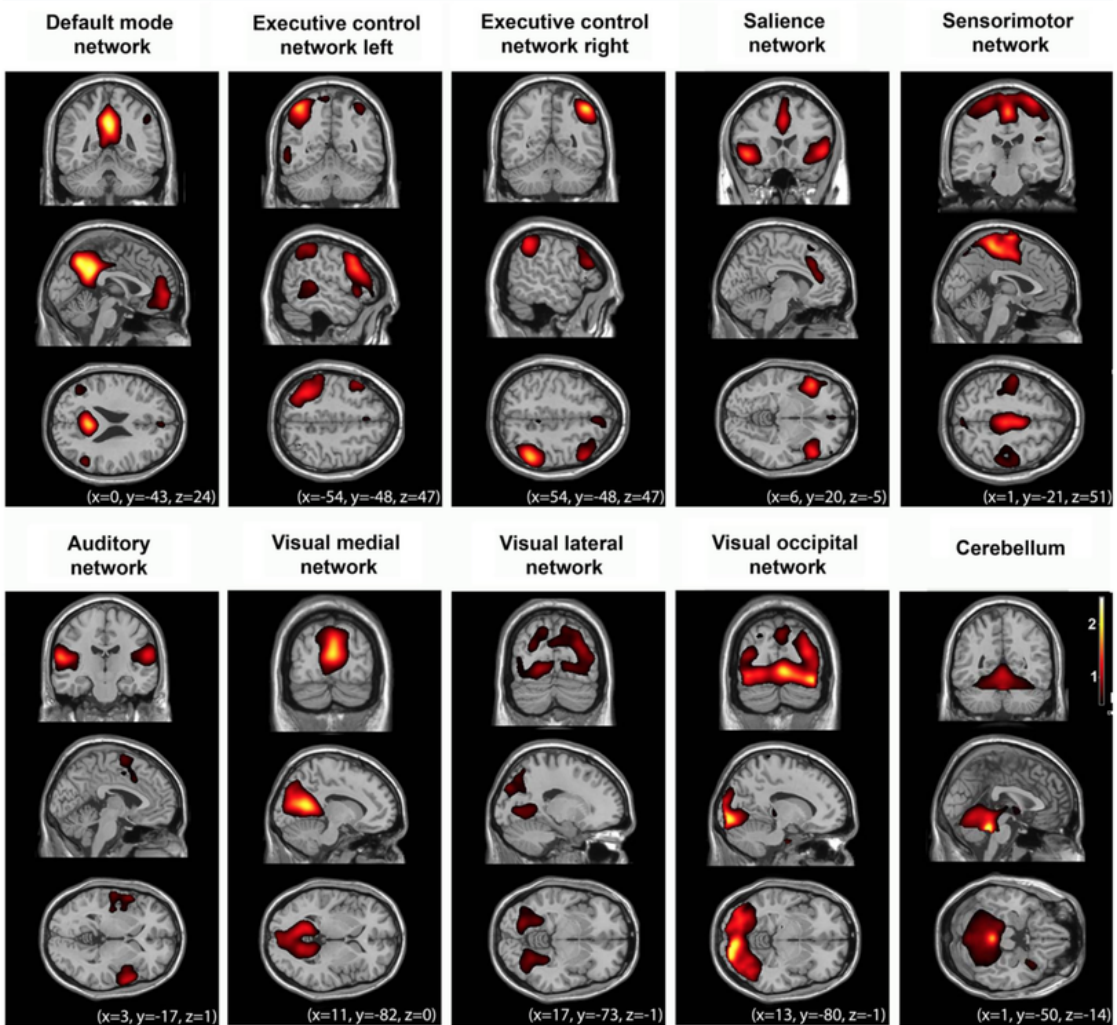


Figure 1.1: Large scale networks identified by performing independent component analysis on fMRI data. Source: Heine et al., 2014

FC between nodes of the salience network with age and correlated this change with a significant decrease in cognitive scores [41]. In another study, although no significant effects of age on FC were found in executive networks, parts of the network FC could predict age-associated change in executive function [42].

The disparity in these results can be attributed to some limitations associated with the study designs, which differ in many aspects. One of the significant differences is the method used to characterize these resting-state networks (RSNs). While some studies use a theory-based approach of defining RSNs like seed-based correlation and graph theory, others have taken a more data-driven approach. The samples used are

also variable across studies, spanning different age ranges and study designs (longitudinal versus cross-sectional). Finally, there are differences in statistical methodology across these studies; while some studies used age regression, some have explored differences between different age groups. Nevertheless, the differences in network-level connectivity across the lifespan have given us a better understanding of the immense capability of the brain to reorganize itself functionally.

1.3 Spontaneous brain activity

Resting-state networks are well established in neuroimaging to show temporally correlated spontaneous activity. Complex thought and behavior arise through the dynamic recruitment of these large-scale brain networks. Previous studies have used different approaches to describe these so-called ‘transient networks’, some of which are described below:

1. **Independent Component Analysis (ICA):** ICA is a method of explorative data analysis which can produce a number of spatial maps and their corresponding time courses when used with fMRI data. Spatial ICA has been found to characterize resting-state brain networks reliably and robustly at both group, and individual levels [43]. A predefined template or atlas is used to perform spatial correction and to identify meaningful neurophysiological spatial components [44]. It can utilize the entire spatial extent to identify large scale networks as well as fine-grained networks by decomposing the functional data into spatial components. According to the model order, larger networks can split into subnetworks by increasing the number of ICs. ICA provides a reliable approach for measuring functional connectivity in the brain, which has been used in previous studies in the context of clinical populations and perception tasks.
2. **EEG Microstates:** In this approach, global patterns of dynamically recurring scalp potential topographies are used to define large scale brain networks called ‘microstates’. The potential maps remain stable for 60-120ms before rapidly transitioning to a different stable topography. Spatial cluster analysis based on k-means clustering or agglomerative hierarchical clustering is popularly used to define the topographical maps at each timepoint [45]. This method, however, can identify a maximum of four to seven cluster maps to optimally describe the data.

3. **Graph theory:** The graph theoretical approach models the brain networks as a mathematical representation of a network, which reduces the complex brain activity to nodes and connections between them. Functional connectivity between networks is modeled in a mathematical framework as pairwise communications between elements.

Nevertheless, the characterization of these networks through indirect hemodynamic response via BOLD signals poses a significant limitation in our comprehension of spontaneous activity. fMRI studies preclude understanding how the low-frequency fluctuations typically associated with RSNs can relate to the much faster timescales of cognition and sensory processing, thus restraining our ability to study the rich temporal dynamics of the underlying electrophysiological activity [46]. Using imaging modalities that directly measure neuronal activity at high temporal resolution is an effective way of overcoming this limitation. EEG and MEG studies have shown that functional connectivity within whole-brain networks exhibits temporal variability on a seconds timescale [47, 48]. However, this temporal resolution is also limited by the length of the sliding time window used to study the inter-regional correlation between time series [49]. Each window requires large amounts of data, ranging from 2-10 seconds in length [50]. The length of the time window chosen limited the visibility of either graphical networks or fast timescale reorganization. This leads to a loss of potentially valuable information about how networks can rapidly reorganize and coordinate in the brain. To this end, Baker et al. [51] used MEG data to develop a distinct methodology based on a hidden Markov model to infer a number of discrete brain states that recurred at different points in time. This approach was not unencumbered by prior assumptions about brain areas or timescales involved. Inferred states corresponded to a unique pattern of spontaneous whole-brain activity underpinned by rapid fluctuations in the 100-200ms timescale, providing a generalized way to study spontaneous brain activity meaningfully. In the subsequent sections, we will go into a brief overview of the model itself and the studies on transient brain dynamics using the model.

1.3.1 Hidden Markov Model

A Hidden Markov model is a probabilistic, statistical model used to derive information from an observable, sequential process that, in turn, is influenced by certain ‘hidden’ or unobservable states. The invisible or hidden states follow a Markov chain (named

after mathematician Andrey Markov). The probability of an event is modeled to be dependent only on the state attained in the previous event.

The example shown in Figure 1.2 shows a simple Markov chain in which there are three states that represent the weather of that day, cloudy, rainy or sunny. Knowing the current day's weather allows us to predict how the weather will be on the next day. The percentages show the probability of state transitions given the current state. A Markov chain can be thus explained as a process with a finite number of states, in which the probability of being in any state is dependent only on the previous state.

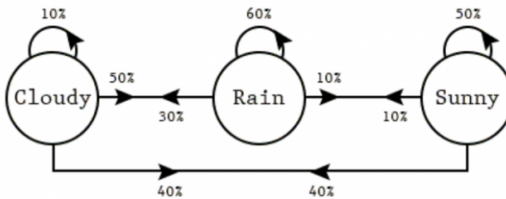


Figure 1.2: An example of Markov chain. Source: [kdnuggets.com \(Markov chains\)](http://kdnuggets.com/markov-chains)

There are two types of probabilities associated with the state changes in a Markov chain - transition probabilities and emission probabilities. Figure 1.3 shows the process of predicting whether a person will be found walking, shopping or cleaning on a particular day, depending upon whether the day is rainy or sunny. In the example, there are two hidden states, rainy and sunny. These are considered hidden because the observable process outputs are whether a person is shopping, walking or cleaning. The start probability represents an initial probability of any day being rainy or sunny. **Transition probability** represents the transition of one state (sunny or rainy) to another state, given the current state. In this example, the probability of transitioning from rainy to sunny states is 0.3, given that the current state is rainy. It also includes the probability of persisting in the same state, which is 0.7 in the case of the current day being rainy.

Emission probability represents the probability of observing the output (shop, clean, or walk) given the current state. So, if the current day is sunny, the probability that a person will be found cleaning is 0.1. What is most important to note is that the process does not depend on any of the past or future states and is independent of the path taken by the past state transitions.

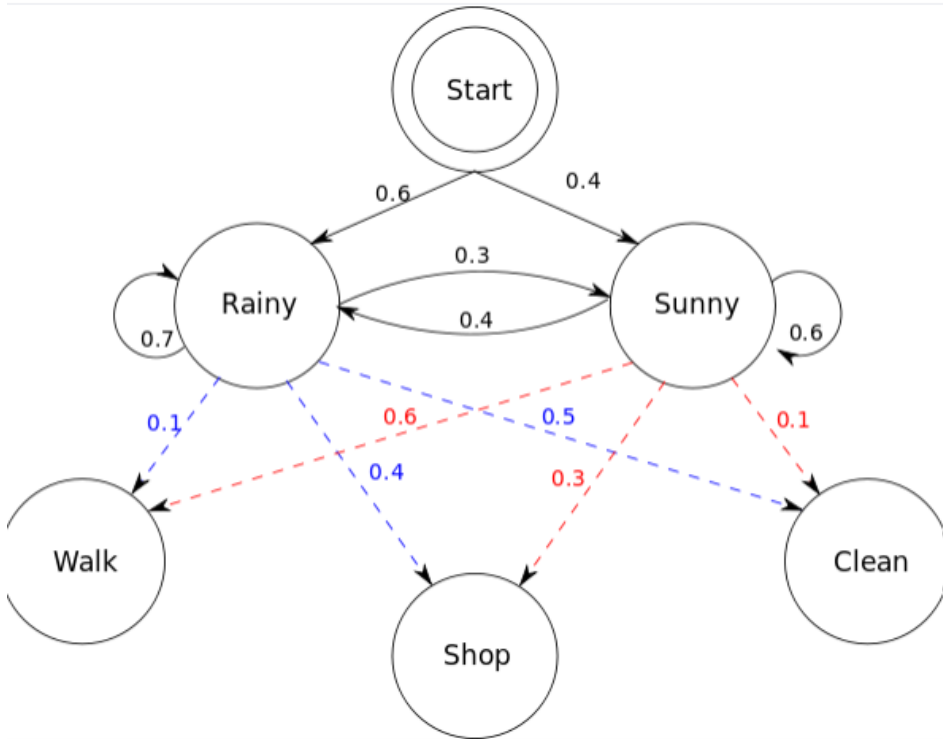


Figure 1.3: Example of Hidden Markov Model. Source: vitalflux.com (Data Analytics)

HMMs have been used in neuroscience in various studies to understand behavior, neuron assemblies, song-learning in birds, stimulus-response relationships, functional dynamics, and brain connectivity.

1.3.2 HMM in transient brain dynamics

Since the pioneering study by Baker et al. [51], many studies have employed HMM to study dynamics in spontaneous neural activity in large-scale transient brain networks. States resembling fMRI RSNs were seen to exhibit inter-network correlations even at fast time scales. For example, the well-established phenomenon of anticorrelation of DAN activation with DMN activation was evident from the low transition probabilities between these two networks. Vidaurre et al. [52] combined HMM with the multivariate autoregressive model to make the model capable of capturing multivariate interactions between brain regions. In this model (HMM-MAR), the observed data corresponded to a MAR model. Each state was related to a unique set of multi-region autoregression coefficients, which describes the neural oscillations. The HMM-MAR model could

thus characterize patterns of oscillatory activity that varied across time, frequency and spatial location. They used task-related MEG data from a volitional motor task to study state-specific spectral properties, namely coherence, power spectral density and partial directed coherence and built time-frequency representations of the same. They could capture fast dynamical changes at the level of coherence and partially directed coherence that was not previously possible using sliding window techniques. In another study by this group, they applied a novel variety of HMM-MAR with embedded time lags to detect changes in phase locking. The new model, TDE-HMM, modeled the neural activity over a particular time window using the covariance matrix. They found specific phase-locking connectivity in the characterized states. The anterior and posterior higher-order cognitive areas corresponding to DMN were found to operate in different frequency ranges [53]. For the anterior-cognitive state, phase-locking was dominant in the delta/theta frequency ranges. On the other hand, the connectivity in the posterior state was dominated by the alpha frequency range. Quinn et al. [50] used the amplitude envelopes of time-courses to infer spatial patterns of amplitude correlations and parallelly used TDE-HMM on raw time-courses. They showed that rapid switching between brain networks could be estimated without knowledge of any task parameters or timings using HMM. It can provide a rich understanding of how the brain reorganizes large-scale networks when performing a task. TDE-HMM was also found to be more sensitive to spectral content and can explain phase relationships between regions and task structure at a higher temporal resolution. A general schematic of the analysis pipeline used in that study is shown in Figure 1.4, which was also used in the current study. The networks have also been seen to have a temporal organization, and the brain networks tend to cycle within two sets of states or metastates [54]. This suggested that the transitions between states are stochastic but not entirely random, and certain networks are much more likely to follow others temporally. Further, the time spent visiting each state (fractional occupancy) was also found to be non-random, which could also be linked to subject-specific behavior. In a recent study, Tibon et al. (2021) [8] applied HMM to resting-state MEG data from Cam-CAN and tried to identify how the temporal characteristics of the states related to cognitive tasks. They used canonical correlation analysis (CCA) to find the relationship between age and performance on thirteen cognitive tasks to assess five broad cognitive domains - executive function, memory, language, processing speed and emotion processing. They found longer occurrences of states involving frontotemporal, higher-order visual and sensorimotor states and shorter occurrences of early visual states in older adults. Even

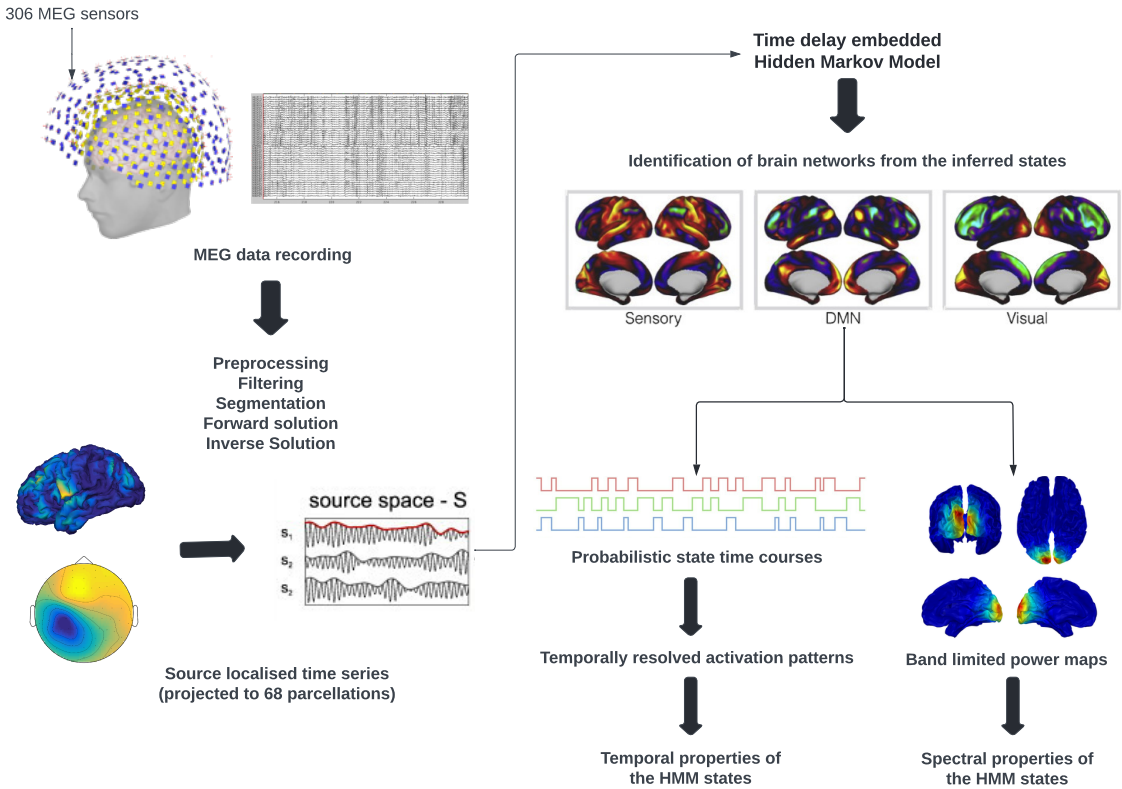


Figure 1.4: General schematic of the analysis pipeline used in employing time delay embedded HMM to source reconstructed MEG data.

though their analysis did not explain much variance in the cognitive data (about 24% combined variance explained), they found significant correlation between twelve of the CCA modes with the temporal characteristics of the HMM states. They also related the greater occurrences of higher-order states to worse task performance and consequently lowered fluid intelligence.

1.4 Scope of dissertation

The effect of aging on cognition is a multifaceted, multimodal phenomenon that takes various factors into account. The age-related changes in functional network dynamics are well established; however, methodological differences have hindered a complete understanding of how the brain networks reorganize themselves with age. Previous studies have successfully characterized resting-state networks using HMM on neuroimaging

data. We wanted to focus on understanding age-associated differences in these transient networks and gain interesting perspectives on whether the established effects of compensatory mechanisms can be seen in a faster, sub-second (100-200ms) timescale. Our hypotheses were as follows:

1. We computed the activation in each state based on functional connectivity to get spatial maps of activity patterns. We expected to find age-related differences in these activation maps and the activation pattern in each state with age. We also expected to see a difference in overall activation values in each state for each age group and across age groups.
2. We hypothesized that there would be differences in certain temporal measures in the transient states with age. We hoped to see decreases in fractional occupancy correlations of anterior and posterior states with an increase in age. We looked at state-wise, age-related differences in transition probabilities, fractional occupancy, fractional occupancy correlation, state switching rates, and mean lifetimes. We wanted to check if these measures can provide an insight into the activation or deactivation of states.
3. We computed frequency band thresholded spectra for all groups. We hypothesized that there would be decreased global coherence as we go from younger to older ages. We also looked for significant clusters of higher power, and wanted to see if the cluster-based coherence or phase lag is more important in driving the age-related changes in connectivity.
4. Finally, we investigated the changes in within-network connectivity in frequency band-limited spectra. We also hypothesized that there would be a reduction in coherence between anterior and posterior regions within a particular state with age. We also wanted to know if frequency plays a role in the connectivity between significant brain regions within a network and if the connectivity pattern can give us an insight into the adaptability of the underlying large scale brain networks in advanced age.

Chapter 2

Materials and methods

2.1 MEG Analysis

2.1.1 Participants

The study used resting-state MEG data from the CamCAN repository (available at <http://www.mrc-cbu.cam.ac.uk/datasets/camcan/>). The dataset is from a large-scale, multimodal, cross-sectional adult lifespan (18-88) population-based study. In the first stage of the study, 2681 participants went through general cognitive assessments at their homes. This population was further screened for poor vision, hearing and neurological disorders, after which around 700 participants were recruited for the second stage, and the rest were excluded from further participation. All screened participants were tested at the Medical Research Council (United Kingdom) Cognition and Brain Sciences Unit (MRC-CBSU) in Cambridge [55, 56].

2.1.2 Data Acquisition

In a light magnetically shielded room, MEG data were collected using a 306-sensor (102 magnetometers and 204 orthogonal planar gradiometers) VectorView MEG System by Elekta Neuromag, Helsinki at MRC-CBSU. Data collection was in compliance with the Helsinki Declaration and was approved by the local ethics committee, Cambridgeshire 2 Research Ethics Committee. The data was sampled at 1kHz with a high pass filter

of cutoff 0.03 Hz. Four head-position indicator (HPI) coils continuously monitored the participant's head position inside the MEG helmet. Two bipolar electrodes were used to record horizontal and vertical electrooculogram signals to monitor eye movements and blinks. Electrocardiogram signals were recorded using another pair of electrodes to facilitate the removal of pulse-related artifacts. The resting-state data used in this study required the participants to sit still with their eyes closed for a minimum duration of 8 min and 40 s.

2.1.3 Source Reconstruction

From the original data, 200 subjects were randomly selected for source reconstruction analysis. Fifty participants from each of the following age groups - Young (18-34 years), Early Middle (35-49 years), Late Middle (50-64 years), and Old (65-88 years) were sampled to ensure homogeneous sampling. Repeated random selections were performed until a relatively equal split between genders was obtained across each age group. The data were preprocessed to remove noise from HPI coils, environmental sources and continuous head motion correction. Max filtering was used to remove the main frequency noise (50 Hz notch filter). The data was then referenced to a standard template (Collins27) [57]. MRI segmentation was performed using Freesurfer, and the boundary element method was used to compute surface triangulation for forward computation. Standard low-resolution brain electromagnetic tomography (sLORETA) was carried out in MNE-python for source estimation. Source time-series were epoched in 5s bins, downsampled to 90 HZ, and projected to 68 brain parcellations according to the Desikan-Killiany atlas [58].

2.2 Data for hidden Markov modeling

2.2.1 Preprocessing

The source time series of all subjects in each group were permuted to yield matrices containing a number of time points by a number of regions elements. Time-points corresponding to the first 1 minute of data was extracted and concatenated across participants of each group. All subsequent preprocessing was performed using the

HMM-MAR toolbox [52]. The data was bandpass filtered between 0 and 40 Hz using a Butterworth filter. To remove strong trends commonly seen in MEG data, a smooth low-order polynomial function was fit to the data and then subtracted from it. This removed the linear trends in the data for each channel and trial separately. The data was then standardized to ensure all trials and channels had the same mean and standard deviation. Since source reconstructed MEG data is associated with a strong artifactual correlation between proximal sources, a symmetric orthogonalization method proposed by Colclough et al. (2015) [59] was used to remove artificial correlations. This was required to reduce the effects of volume conduction due to signal leakage before any functional connectivity estimation could be performed.

2.2.2 Source reconstructed dipole ambiguity

One prevalent issue when dealing with source-reconstructed M/EEG data is that the estimated source data has ambiguous signs due to vague source polarity. The signs of the reconstructed dipoles may be inconsistent across subjects, which can lead to suppression of group-level phase relations between two brain regions [50]. The sign flipping algorithm described by Vidaurre et al. (2018) [53] was used on the data to find the best combination of flips for our data. This flipped data was used further in all our analyses.

2.2.3 Time-delay embedded Hidden Markov Model

A Hidden Markov Model (HMM) has been shown to be useful in flexibly characterizing dynamic data into a set of discrete functional states that reoccur over time. The dynamics in the brain can be represented as a system moving through distinct hidden states, which are mutually exclusive, i.e. at one time point, only one state is active. However, since HMM is a probabilistic model, the inference process assigns a probability of being active to each state at each time point. For a Markovian process, this probability of a state being active at any time point t , depends on which state was active at time point $t-1$ (order-one Markovian) (see Figure 1.2 for more details). It is important to note that the states are hidden and not directly observable from the raw data; thus the model assumes that data observed in each state are drawn from a probabilistic observation model. When the system is in a particular state, the observed

data is drawn from that state's observation model (with its own model parameters), which defines a probability distribution. For this study, we used a type of HMM that allows us to detect changes in both power and phase. Using this approach, the observation distribution is described as the neural activity over a particular time window using a Gaussian distribution with zero mean [53]. Essentially, the covariance matrix is used to model the autocovariance (lagged cross-covariance) across regions during that time window. For the time points in which a particular state is active, the model can effectively capture patterns of linear synchronization and thus can describe state-wise phase-locking. The source time series for each region was embedded with fifteen time delay lags (-7 to 7). PCA was performed on the embedded data to avoid overfitting and reduce the computational load. The number of principal components is responsible for determining the range of frequencies that are available to the HMM. As PCA tries to explain the highest possible amount of variance in the time-series data, and the power or variance of the electrophysiological data is most concentrated in slower frequencies (1/f nature), a total of 136 components (twice the number of regions) were used to allow the model to be sensitive to higher frequencies as well [51].

2.2.4 Similarity between inferences

The HMM was run multiple times, and the result of each iteration was qualitatively compared. The statistical dependence between the state time courses between two runs can measure the similarity between two HMM inferences. Out of ten runs, the HMM result with the lowest free energy and highest similarity with other runs was selected for further analysis.

2.2.5 Age-wise group HMM estimation given state course probabilities

Since we wanted to see age-related differences in transient state dynamics, we used the HMM results obtained from running the inferential process on the entire data and re-inferred the states to attain group-specific states. The data was previously standardized using the entire data set so that the properties of the group-specific data do not change drastically with respect to the rest of the data. The HMM inference

was then run separately for all four age groups (Young, Early-Middle, Late-Middle and Old).

2.3 Resting State Temporal Dynamics

From the estimated probabilistic state time courses, we compared several measures of temporal dynamics of these transient brain states across age groups. The main temporal features we investigated include:

2.3.1 Transition Probabilities

To assess the relationship between different functional networks, the transitions between inferred states was calculated as the probability of transitioning to any other state, given the current state (without considering persistence probabilities).

2.3.2 Fractional Occupancy

Fractional occupancy (FO) is the proportion of time spent by the system in each state. Assuming any state is either on or off at any time-point (hard classification by choosing the most probable a posteriori state), fractional occupancy can be calculated as:

$$\text{fractional occupancy } (k) = \frac{1}{T} \sum_t (u_t == k)$$

where, $u_t == k$ is one if $u_t = k$ and is zero otherwise, k is any state and T is the length of state sequence in samples. FO and FO correlation between states were compared across all age groups to study cross network interactions.

2.3.3 Dwell Times

Dwell time or state lifetime is the average amount of time spent in each state before the system transitions out of that state. The dwell time of a particular state reflects

the temporal stability of the states.

$$\text{mean life time } (k) = \frac{\sum_t (u_t == k)}{\text{number of occurrences } (k)}$$

where, the *number of occurrences* is given by:

$$\text{number of occurrences } (k) = \sum_t (((u_t == k) - (u_{t-1} == k)) == 1)$$

2.3.4 State switching rates

State switching rates provide a measure of stability per subject for each session or trial. This provides a group level measure of the average switching rates between all states for that particular age group.

2.4 Spectral Statistics

2.4.1 Spatial activation maps

Custom scripts from OHBA Software Library (OSL) were used to visualize the state-wise activation pattern in brain space. The first eigenvector of the covariance matrix was taken as a measure of functional connectivity between brain regions. Custom scripts were written in MATLAB to map voxel-level activation to corresponding parcels automatically. The activated brain regions in each state were compared across age groups and categorized into networks resembling fMRI resting-state networks.

2.4.2 Non-parametric estimation of state spectra

Since the HMM estimation of state time-courses did not employ any MAR order or fixed sliding window length, we used a non-parametric, state-wise multitaper approach proposed by Vidaurre et al. (2016) [52] to obtain the states' spectral information without any PCA-induced bias. The inferred HMM state time courses are used as temporal windows to estimate state-specific spectral properties using a weighted version of the multitaper. The non-parametric approach is more accurate and robust as it can

make more efficient use of the data by not constraining the temporal resolution of the changing patterns of the neural data.

2.4.3 Change in global coherence and phase coupling

We calculated subject-specific global coherence and phase lag index between brain regions in both wideband and narrowband limited frequencies from the state spectra for all age groups as described above. Data-driven spectral decomposition into frequency bands closely resembling classical frequency bands (e.g. theta, alpha and beta bands) was performed using the *spectdecompose.m* function from the HMM-MAR toolbox. This algorithm performs non-negative matrix factorization on the matrix of spectrally defined coherence across all states and pairs of regions. We wanted four components such that we could capture the spectral profiles of the required frequency bands (delta/theta, alpha, beta and low gamma) in the components. After decomposition, the spectral profiles were checked to see if they corresponded to canonical frequency bands (i.e. if the modes had a clear peak) and were re-inferred as required. Since our data were bandpass filtered to have a 40 Hz upper limit, we focused our analysis on the first three components and excluded the fourth (low gamma band) component from further analysis. Wideband coherence and PSD were also computed for all age groups by setting the number of components required to two, corresponding to average coherence and PSD values across all frequency bins. We extracted the clusters which contained higher power than the global average in all states. The clusters common in all age groups were selected for further investigation of within-network, cluster-based analysis of coherence and phase coupling.

2.4.4 Connectivity analysis

To study the connection strength between different brain regions in specific frequency ranges, we used cluster based coherence and PLI values, as described in the previous section. The instantaneous phases obtained from the non-parametric state spectra estimation were averaged across participants in each age group in the theta, alpha and beta frequency ranges. PLI is known to provide a reliable estimate of phase synchronization and is robust against the presence of common sources, and volume

conduction [60]. The PLI was calculated as:

$$PLI_{ij} = | \langle sign(\Delta\phi_t) \rangle |, 0 \leq PLI_{ij} \leq 1$$

Here, the sign function yields: 1 if $\Delta\phi_t = 0$; and -1 if $\Delta\phi_t < 0$.

Coherence and phase-based connectivity were quantified in those specific parcels of the brain depending on the frequency band thresholded power spectra. The significant measures were represented as connection strengths (thresholded to show 50% strongest connections) between brain regions as circular plots [61] depicting nodes on the circumference and lines connecting two nodes to show the connection.

2.4.5 Statistical Analysis

Statistical tools used for quantifying differences between the studied property across age were mainly Two-way analysis of variance (ANOVA) and multiple comparisons of means (using Bonferroni correction). Post-Hoc Tukey's test was used to highlight statistically significant differences between the groups. In most of the comparisons (unless mentioned otherwise), a 4×8 design is used, which considers the main effects of the four age groups and the eight inferred states. The Fisher's F statistic is used to determine the ratio of variances explained by the group means and is calculated as:

$$F = \frac{\text{explained variance or between group variability}}{\text{unexplained variance or within group variability}}$$

$$\text{where, explained variance} = \frac{\sum_{i=1}^K (n_i (\bar{Y}_i - \bar{Y})^2)}{K - 1}$$

\bar{Y}_i denotes the sample mean in the i -th group, n_i is the number of observations in the i -th group and \bar{Y} is the overall mean. K denotes the number of groups in the data.

$$\text{The unexplained variance is} = \frac{\sum_{i=1}^K \sum_{j=1}^{n_i} (Y_{ij} - \bar{Y}_i)^2}{N - K}$$

where, Y_{ij} is the j^{th} observation in the i^{th} out of K groups. N is the total sample size.

All significance measures are performed with an alpha level of 0.05 (95% interval of confidence).

Chapter 3

Results

3.1 The activation pattern of states follows a distinct trend with age

Eight transient brain states were inferred from applying the HMM model to the data for all age groups in a completely data-driven manner. These states reveal unique spatial patterns of functional activity which resembled resting-state networks previously characterized using fMRI techniques. From the inferred states, States 1, 2 and 6 resemble the default mode network while other states resemble sensory networks. The spatial activity patterns of States 3, 4, and 8 resemble the visual networks, and States 5 and 7 resemble frontoparietal networks. However, due to spatial ambiguity in source reconstructed MEG data, an exact match of these states to particular networks was not possible. From here on, we will stick to the nomenclature ‘HMM-States’ to denote the recurrent patterns of activity modeled by the HMM. The covariance matrix of each state over all the lagged time windows used to model the states were used to generate volume and surface activation maps of functional activation. Each of these states described brain activity in terms of power and coherence covariations and is temporally resolved. Figure 3.1 shows the pattern of activation in each age group for states arranged in ascending order. State 1 and State 2 were seen to have higher overall whole-brain activation in all age groups, except in the late middle-aged group, where the brain exhibits the highest functional connectivity in State 8 compared to all other states. Two-way ANOVA performed on the whole brain activation values showed a

significant main effect of state ($F(7, 2175) = 148.19, p < 0.001$) with State 2 having a larger activation ($M = 0.0097, SD = 0.00041$) than all other states. The main effect of age ($F(3, 2175) = 7.22, p < 0.001$) was also significant, with late middle age group showing higher mean activation value ($M = 0.003$). We also found a significant effect of the interaction between states and age ($F(21, 2175) = 101.77, p < 0.001$).

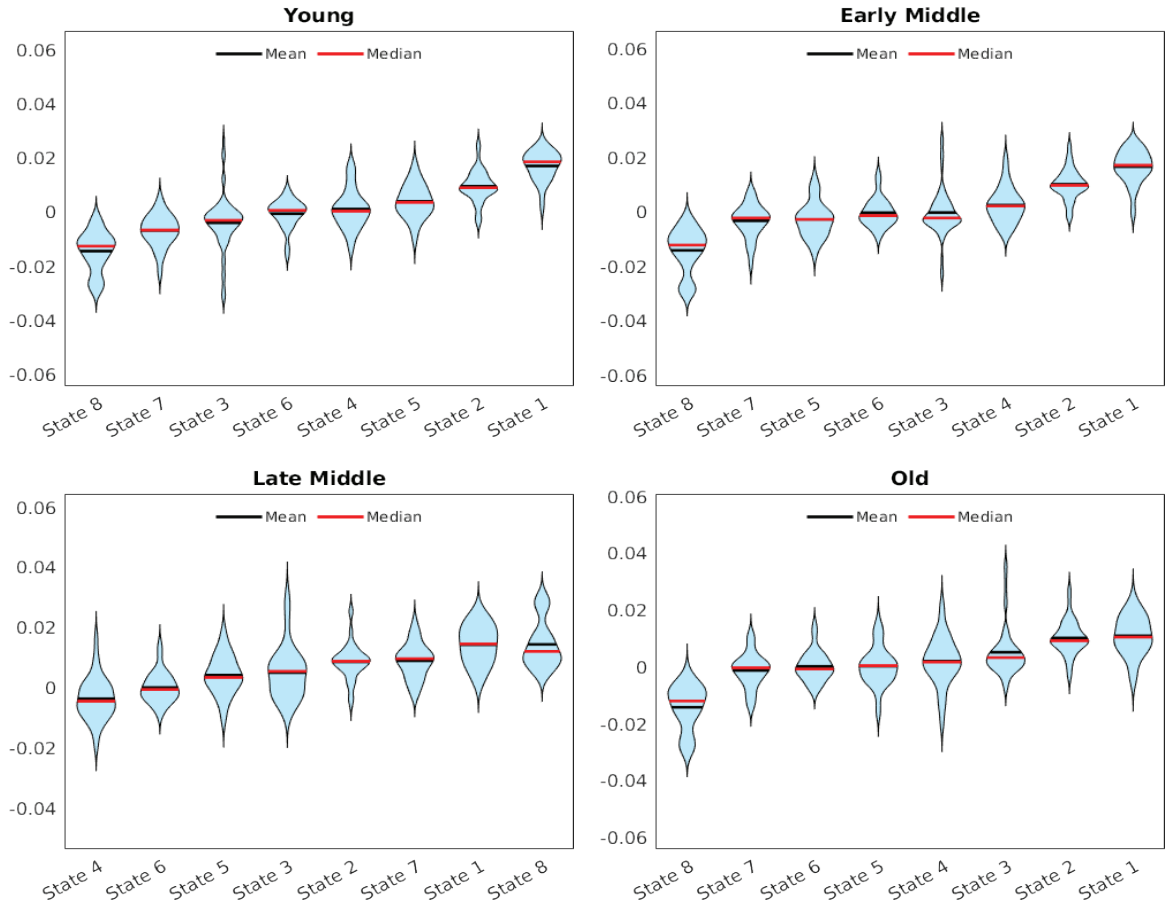


Figure 3.1: Mean activation in each age group: States are arranged in ascending order of mean functional activation in each age group. The red line signifies the mean activation in each state over all brain regions, the black line signifies the median.

All the states were also seen to have spatial activation in both the anterior and posterior regions, with the exception of State 3 in all age groups and State 5 in three of the age groups. Cluster-based statistical testing performed on the common parcels getting activated in all age groups in a particular state revealed the overall trend in the change of activation pattern with age (Figure 3.2). We found a significant effect

of age for all states ($p < 0.001$), except State 2 ($F(3, 51) = 0.47, p = 0.7$). Thus, in State 1, even if the overall mean functional connectivity remains high compared to all other states, there is a decreasing trend with age. This could suggest functional reorganization of the underlying brain networks to keep the overall activation high in particular networks or brain regions to counteract the detrimental effects of aging on cognitive performance. Activations in the clusters of all other states were seen to change non-linearly with age ($p < 0.05$).

The volumetric and surface maps of the activation patterns are shown in Figure 3.3 and Figure 3.4 respectively. We performed Post-Hoc Tukey's test to compare all pairs of means and control the family-wise error rates. All the statistical differences in a pair of states in both whole-brain and cluster-based functional connectivity are summarized in the Tables 5.1 and 5.2.

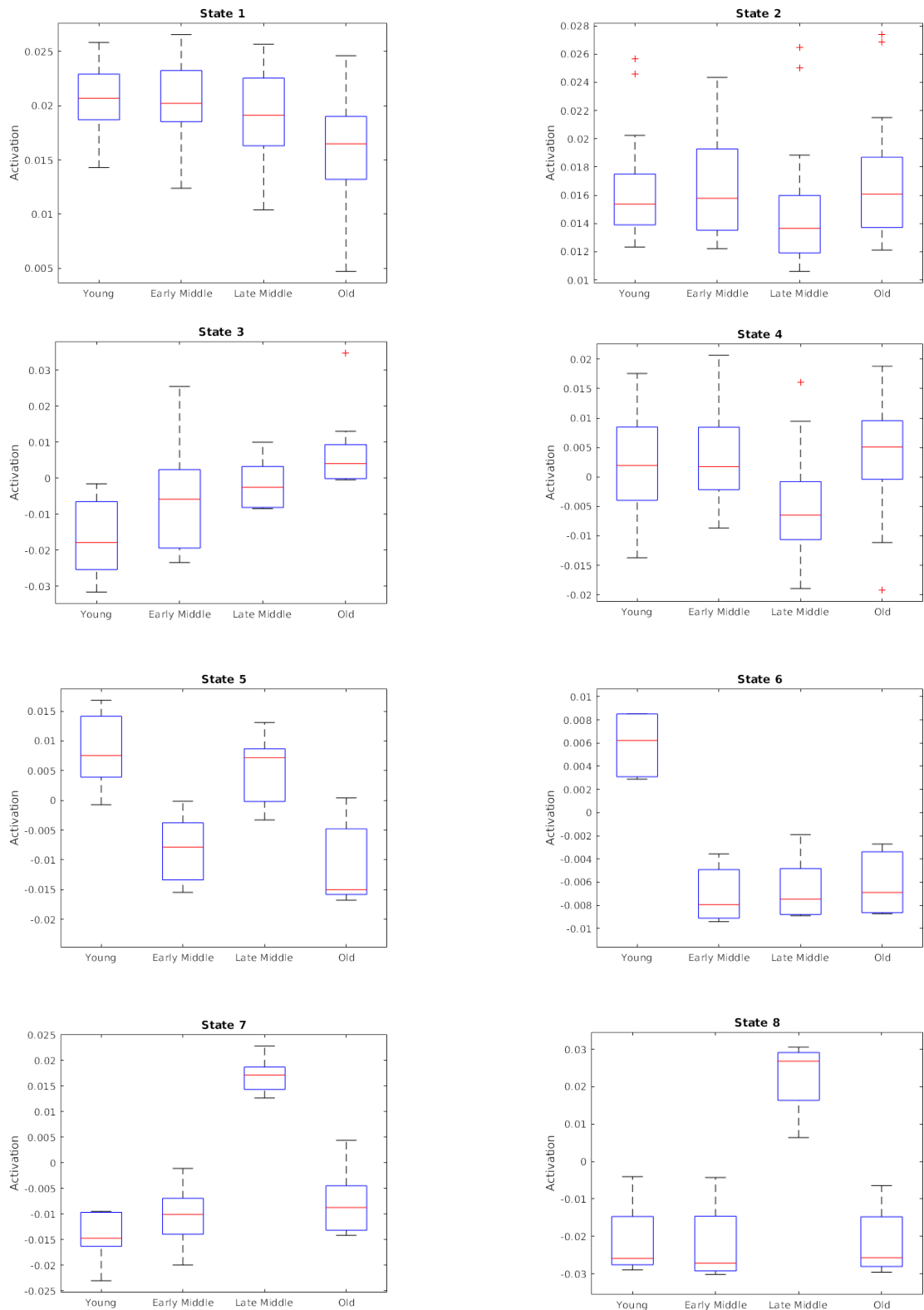


Figure 3.2: Statewise parcel activation compared across age groups: Comparison of the mean activation value in activated clusters or regions in each state across all four age groups. The red line inside each box signifies the mean.

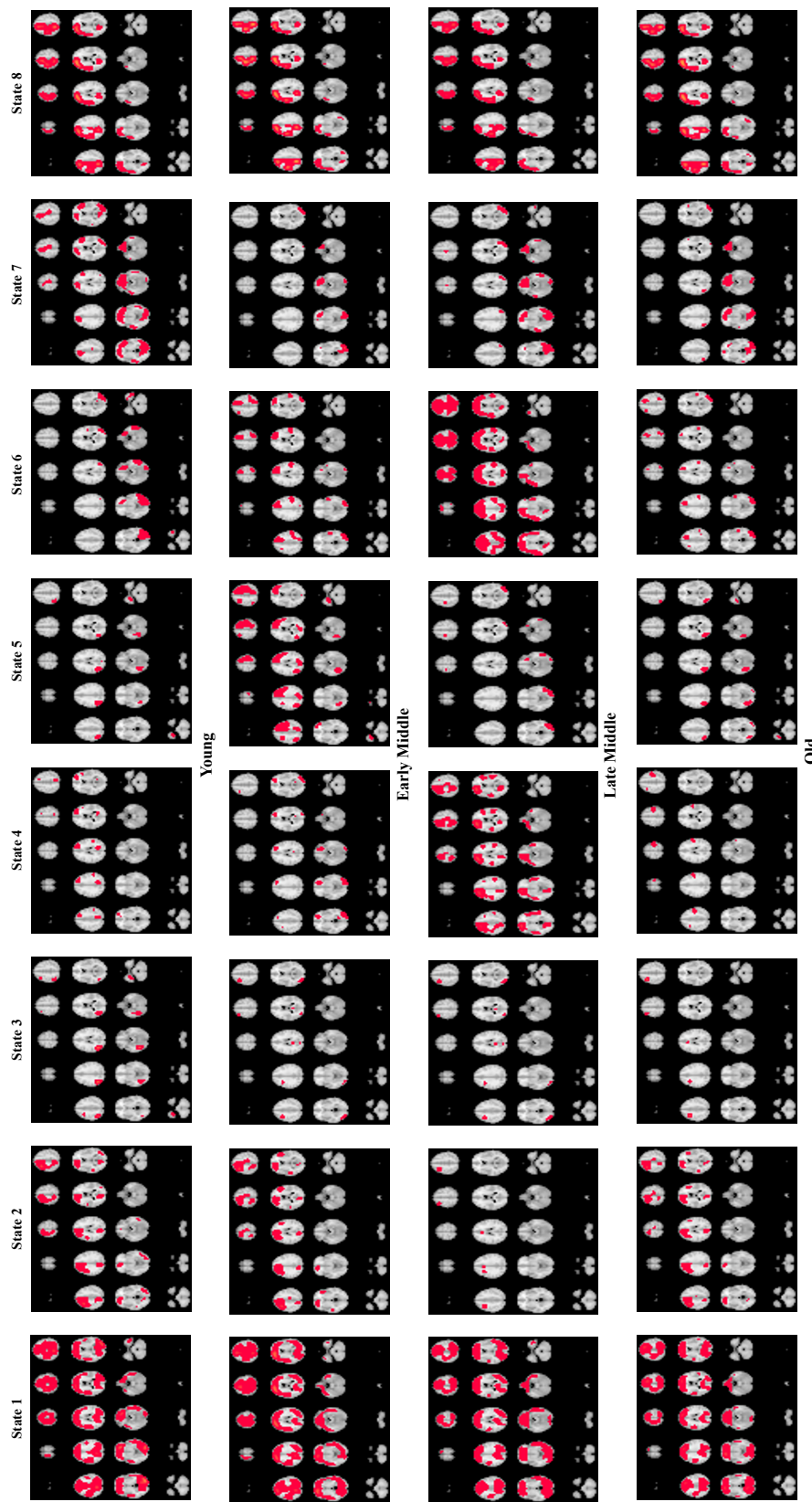


Figure 3.3: Volumetric maps showing spatial activation pattern: Functional connectivity maps showing the spatial activation pattern in all eight states across age groups. Red color signifies higher functional connectivity in those regions compared to the global average.

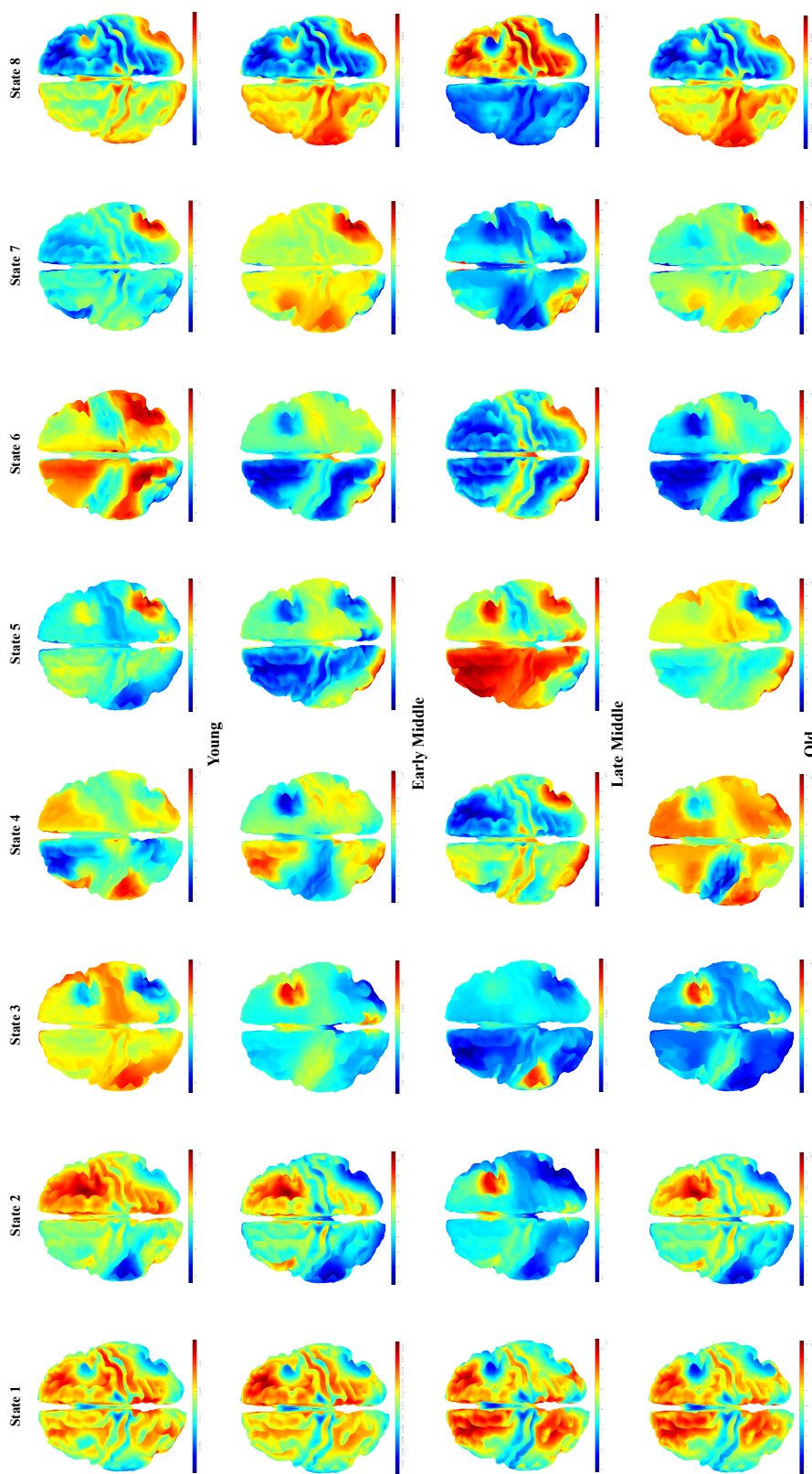


Figure 3.4: Surface maps showing spatial activation pattern: Functional connectivity maps showing the spatial activation pattern in all eight states across age groups. Functional connectivity in the regions higher than the global average show warmer colors (red). Regions showing lower activation than global average are marked with cooler colors (blue).

3.2 Temporal Dynamics

3.2.1 The probability of transitioning between states remain stable with age

The large-scale brain networks or HMM states are described by assuming mutual exclusivity of the states at any time point. However, since the recruitment of states at any time point is the probability of a state being active and not an absolute value, we can utilize the probabilistic state time courses to study transitions between states as a measure of the underlying cross-network interactions and state dynamics. The transitions from the dominant state at any given time point to another state at the next time point for all age groups are shown in Figure 3.5. Two-way analysis of variance revealed a significant main effect of state ($F(7, 255) = 29.86, p < 0.001$). The main effect of age on transition probabilities did not show significance ($F(3, 255) = 7.5\text{e-}30, p > 0.5$) In all age groups, the probability of transitioning to State 6 from any other state was found to be significantly higher ($M = 0.34, SD = 0.02$) whereas State 3 showed the lowest transition probability ($M = 0.008, SD = 0.019$). The pairwise comparisons between the transition probabilities of all states are provided in Table 5.3.

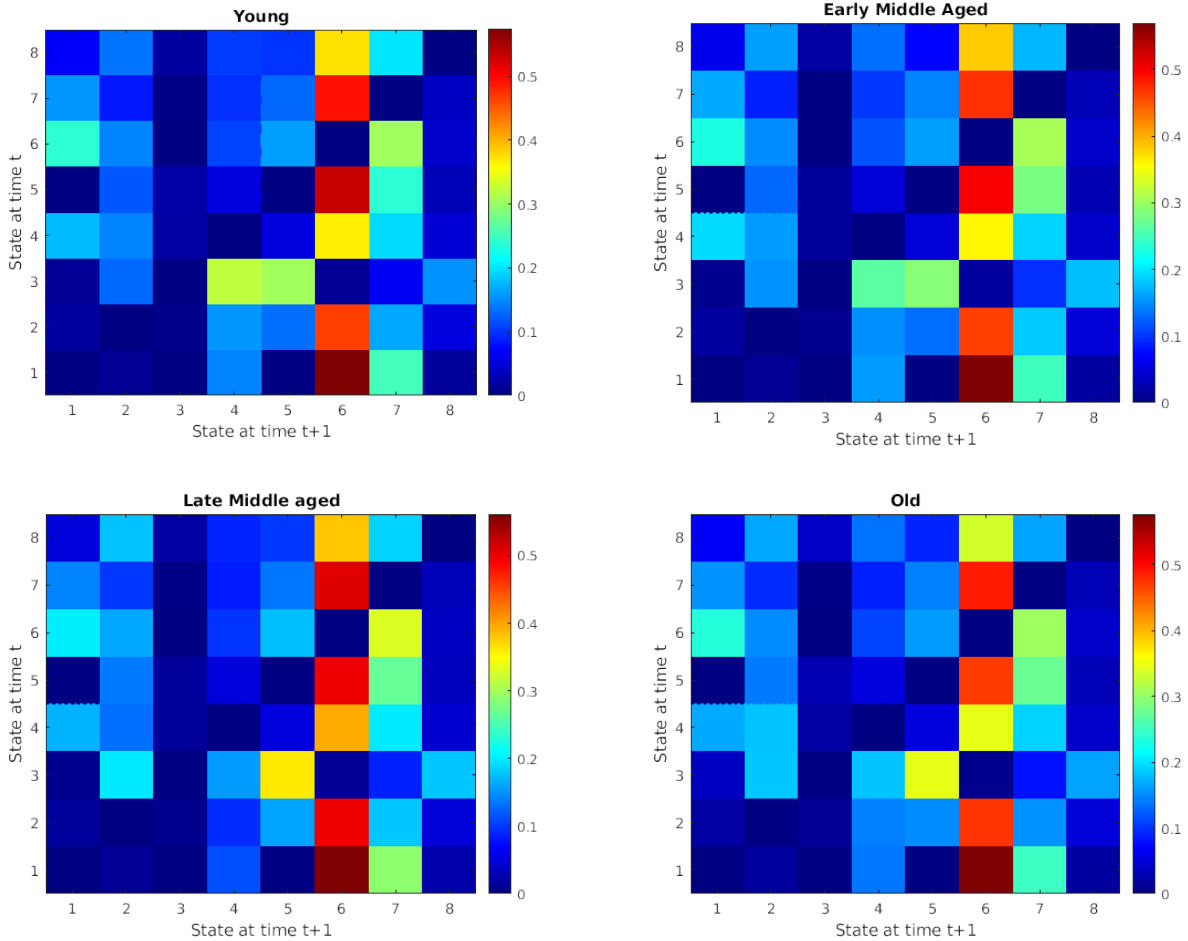


Figure 3.5: Transition probability across all age groups

3.2.2 Fractional Occupancy of states in all age groups

The percentage of trials that a particular state occupies was measured from the probabilistic state time courses as described in the Methods section (see Section 2). State 6 had a significantly higher fractional occupancy in all age groups. This is also supported by the previous result, which shows that there is a higher probability of the brain visiting State 6 from any current state (see Figure 3.5). Two-way analysis of variance yielded a main effect of state ($F(7, 19199) = 1653.4, p < 0.001$), but not with age ($F(3, 19199) = 5.01e-29, p > 0.5$) at the chosen significance level. The significance values, when corrected for multiple comparisons, revealed that in all age groups, State 1 and State 4 are seen to have similar fractional occupancy time windows and do

not differ significantly from each other ($p = 0.09$) in the 95% confidence interval, but reaches significance at the 90% confidence interval. However, the interaction effect of age and state was found to be significant ($F(21, 19199) = 7.41, p < 0.001$).

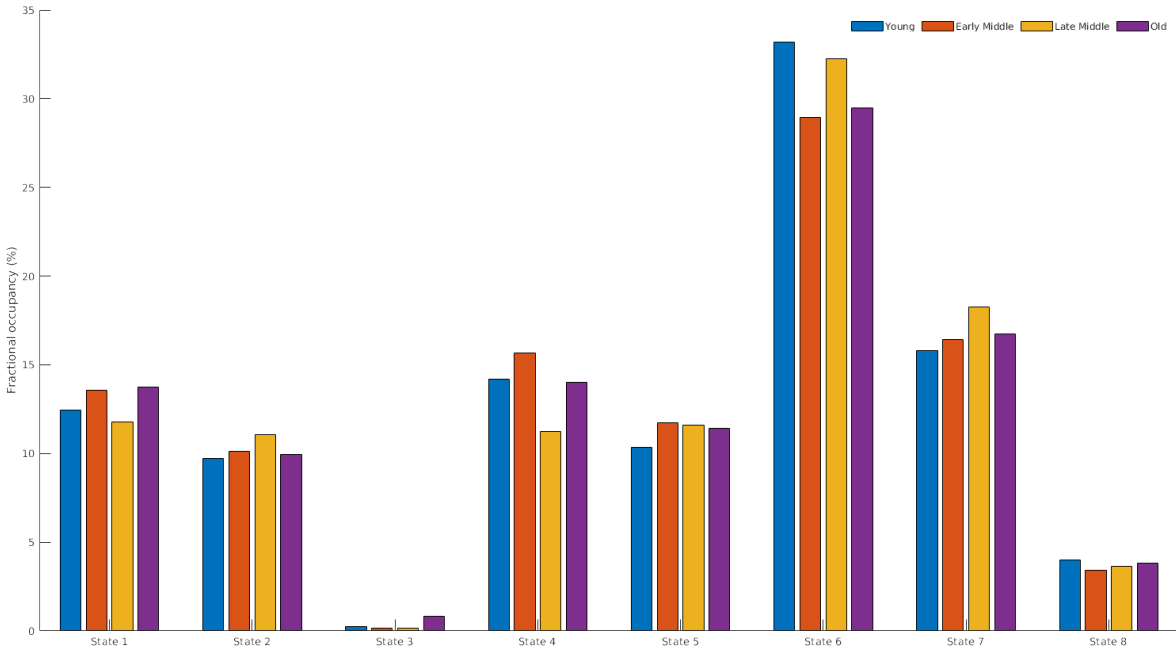


Figure 3.6: Fractional Occupancy of each state across all age groups

The fractional occupancy can also give us an insight into the cross-network connections between each state. The HMM state definition assumes mutual exclusivity within the states and probabilistically chooses the most dominant (most likely to be active) state at any time point. The probabilistic nature of the time courses allows us to study the correlation between the probability of two states being active simultaneously. In a way, this gives us cross-network functional connectivities by allowing us to see which two networks are more likely to get activated together. Conversely, it also allows us to see which networks act antagonistically to each other and rarely get activated at the same time. Statistical tests showed a significant main effect of states on explaining the variability in the data ($F(7, 255) = 3.53, p = 0.001$). The main effect of age and the interaction term were not statistically significant ($p > 0.1$). Post-Hoc Tukey's test showed that State 2 has a larger mean fractional occupancy correlation with other states ($M = -0.02, SD = 0.03$). State 6 was seen to have the lowest mean ($M = -0.17, SD = 0.03$) correlation with other states. The high transition probability of the brain to switch to State 6 is further supported by this result as other states are

not seen to co-activate along with State 6 but rather switch to State 6.

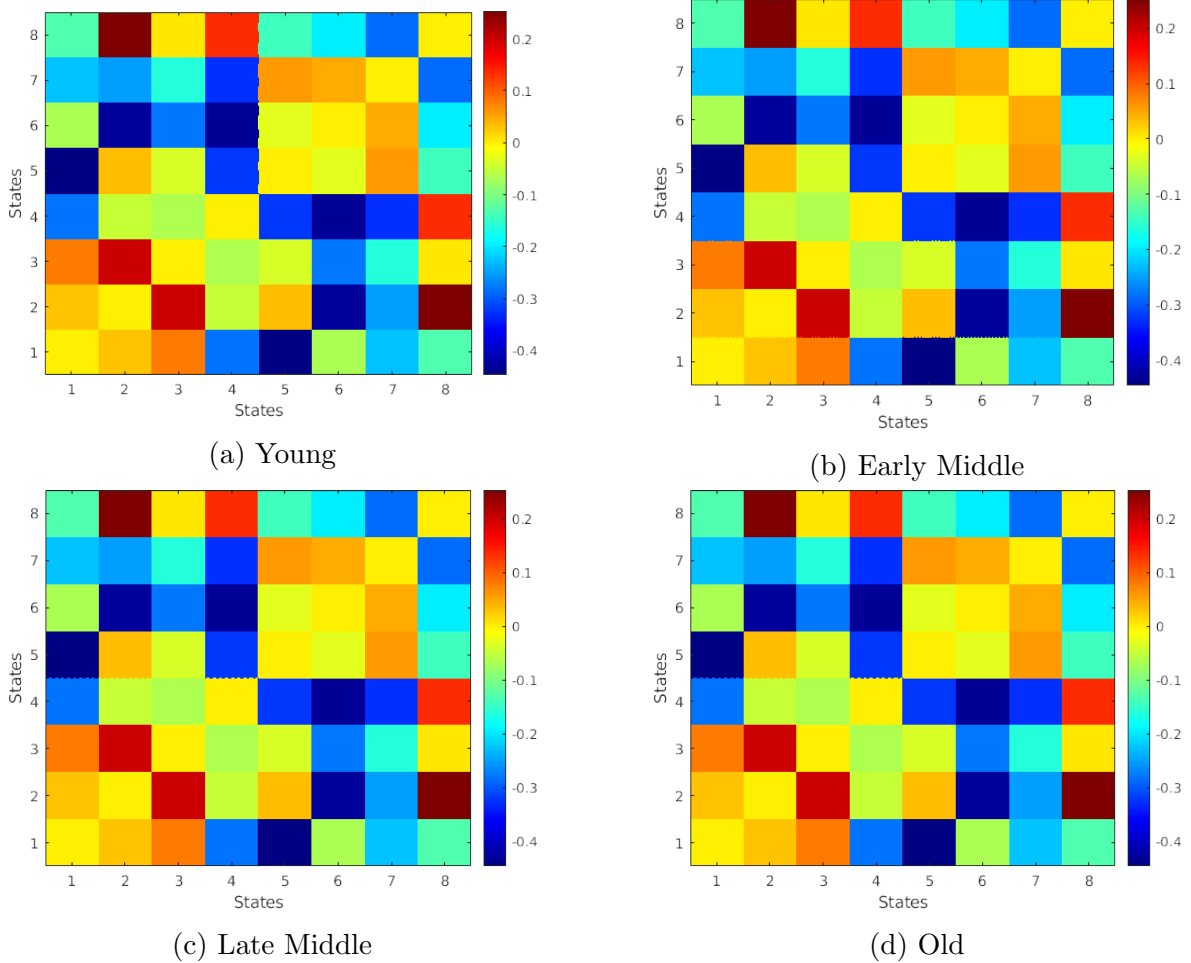


Figure 3.7: Fractional Occupancy correlation: Correlation matrix between the fractional occupancy time courses of each state for a) Young, b) Early Middle, c) Late Middle, d) Old age groups. Positive correlations between states indicate that the two states are visited together more frequently during similar timepoints.

3.2.3 The mean lifetime of a state's activation

The mean lifetimes of the states were calculated by averaging the total number of time points each state spends on a trial. A threshold of fifty time points was selected to define the lifetime at each state visit. Figure 3.8 shows the mean lifetimes of the states in ascending order in each age group. Two-way analysis of variance with age and states

as main effects yielded a significant effect of states ($F(7, 31) = 3.53, p = 0.01$) but not with age ($F(3, 31) = 1.53, p = 0.23$). Corrections for multiple comparisons showed that in all age groups, the mean lifetimes for State 3 ($M = 21.56, SD = 10.3$) and State 8 ($M = 25.5, SD = 10.3$) are significantly lower than all other states. Additionally, State 3 failed to meet the threshold criteria of being activated for at least 50 time points in all age groups except the old group. State 4 had the largest mean lifetime ($M = 68.6, SD = 10.3$) among all states.

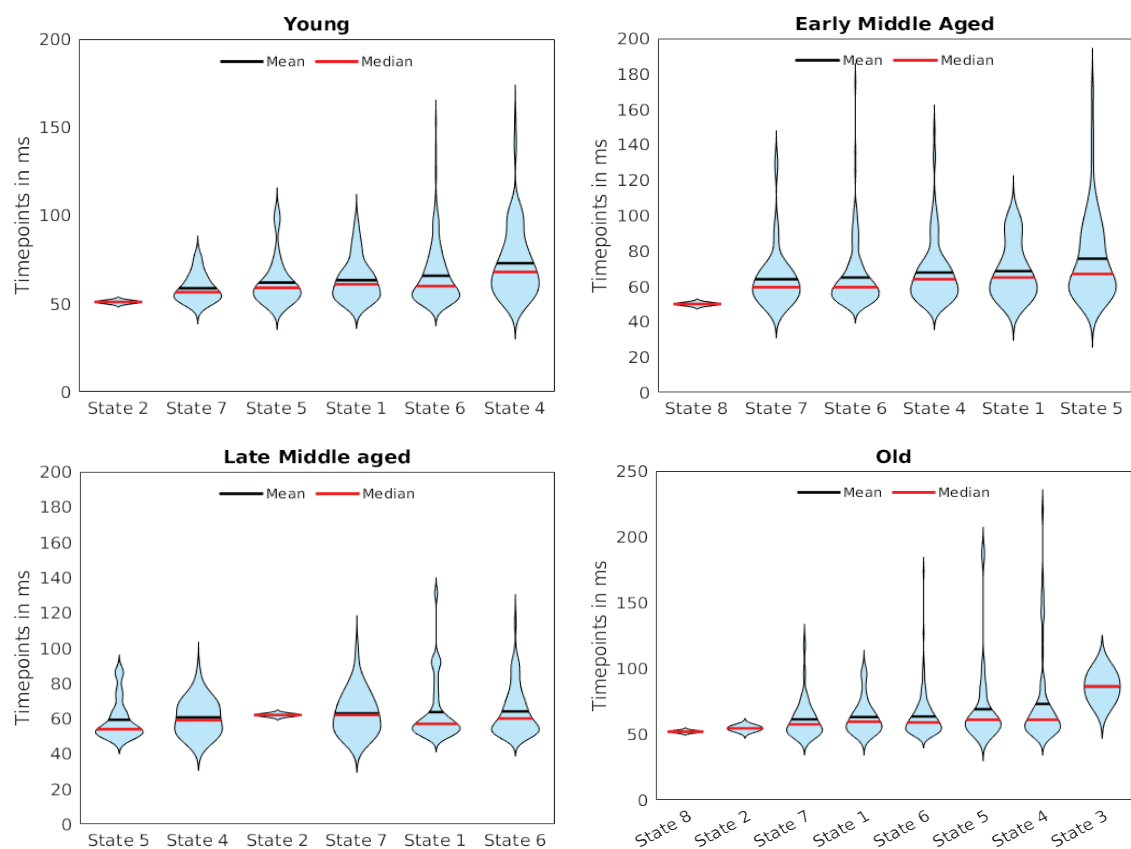


Figure 3.8: Mean lifetimes of the states in each age group. The black line inside each violin denotes the mean of the distribution. The median is indicated by a red line. A higher mean lifetime indicates fewer fluctuations and more stability of a particular state.

3.2.4 State switching rates

The state switching rates provide a measure of the stability of the states in each age group. A subject-wise analysis of the temporal stability of each state revealed that the switching rate of the young and early middle-aged groups differed significantly from the other two age groups ($p < 0.001$). Multiple comparison analyses also showed that there are no significant differences between the state switching rates of young and early middle-aged groups ($p = 0.99$) as well as late middle and old aged groups ($p = 0.22$). The mean state switching rate was found to be higher in the late middle-aged group ($M = 0.075$, $SD = 0.0004$), however, it was not that much higher than the other age groups. Differences between the switching rates of a pair of age groups were quantified after correcting for the family-wise error rate. The young and early middle-aged group had a significantly lower switching rate than the late middle and old age groups ($p < 0.001$).

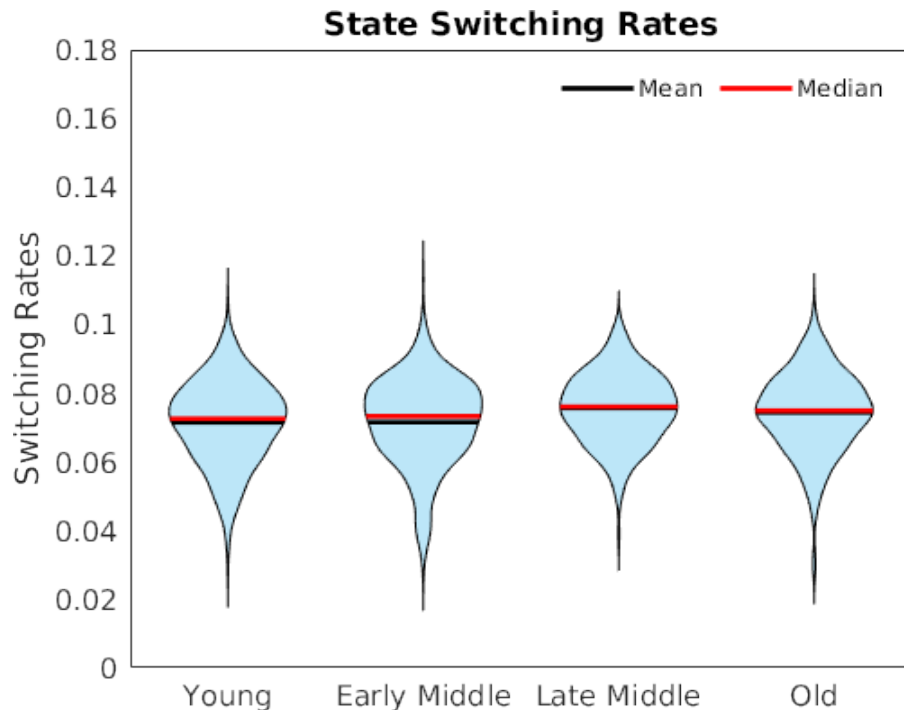


Figure 3.9: Mean state switching rate in all age groups

These measures of fractional occupancies, mean lifetimes of the states and state switching rates together constitute the ‘chronnectome’ of the HMM states.

3.3 Spectral Dynamics

3.3.1 Change in state specific global coherence with frequency

In different frequency bands, large scale functional connectivity between whole-brain networks has been seen to show different power and phase coupling patterns. We wanted to see how the whole brain correlation of power in different states in different frequency bands varies with age. For all age groups, we performed a data-driven decomposition of the whole brain spectral features into specific frequency bands, namely wideband (0.5-40 Hz), theta (0.5-10 Hz), alpha (5-15 Hz) and beta (15-30 Hz). These frequency bands are named based on their resemblance to classical frequency bands, which are not precisely the same as the classical theta, alpha or beta bands. Figure 3.10 shows the spectral profiles of the data-driven decomposition into frequency bands and the corresponding modes of all age groups. In all age groups, the spectral profile looks more or less similar in particular bands and have peaks that correspond to classical frequency bands.

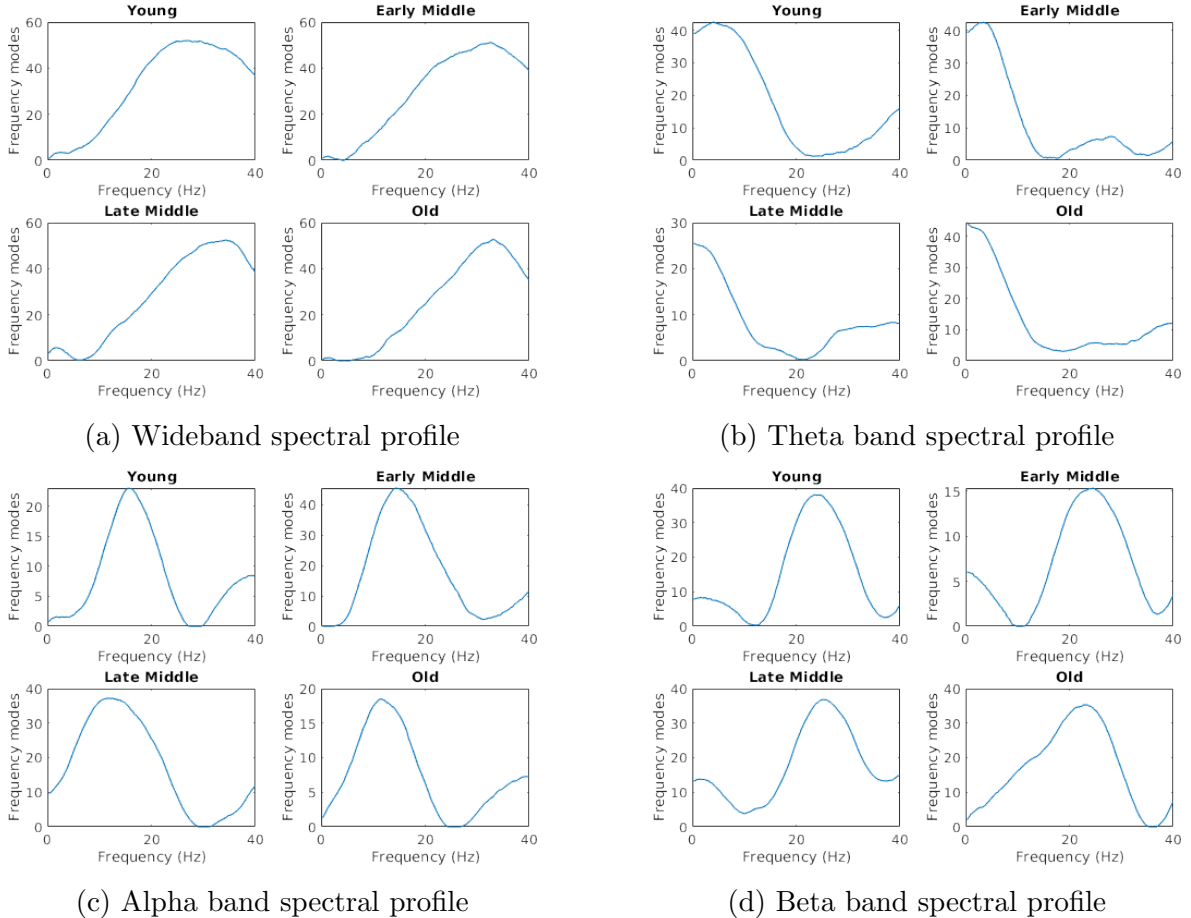


Figure 3.10: Spectral Profile: Data driven decomposition of the spectra in all age groups resulted in the division of a) wideband (0-40 Hz) spectra into three different frequency modes. The peak frequency (modes) obtained in the spectral profiles resembles the classical b) theta (0.5-10 Hz), c) alpha (5-15 Hz) and d) beta (15-30 Hz) ranges in all age groups.

Previous studies have shown that global coherence also increases with an increase in power. We first looked at whole-brain coherence between regions in each state and compared the coherence levels across age groups. In the wideband condition, there is no thresholding of the frequency, and the coherence values are averaged across all brain regions to access the full spectral resolution. On the other hand, for the theta band thresholded global coherence, the coherence between brain regions in the 0.5-10Hz frequency range. Similarly, for alpha and beta band global coherence, the spectra were filtered from 5-15 Hz and 15-30 Hz, respectively. The states were arranged to show lower

to higher average coherence values in each age group. Interestingly, even though the absolute value of coherence changes across age groups, the pattern of global coherence between the states remained the same in a particular age group in all frequency bands. Figure 3.11-3.14 shows the trend of low to high coherence values, and the sequence of states in each age group remains constant in all frequency bands.

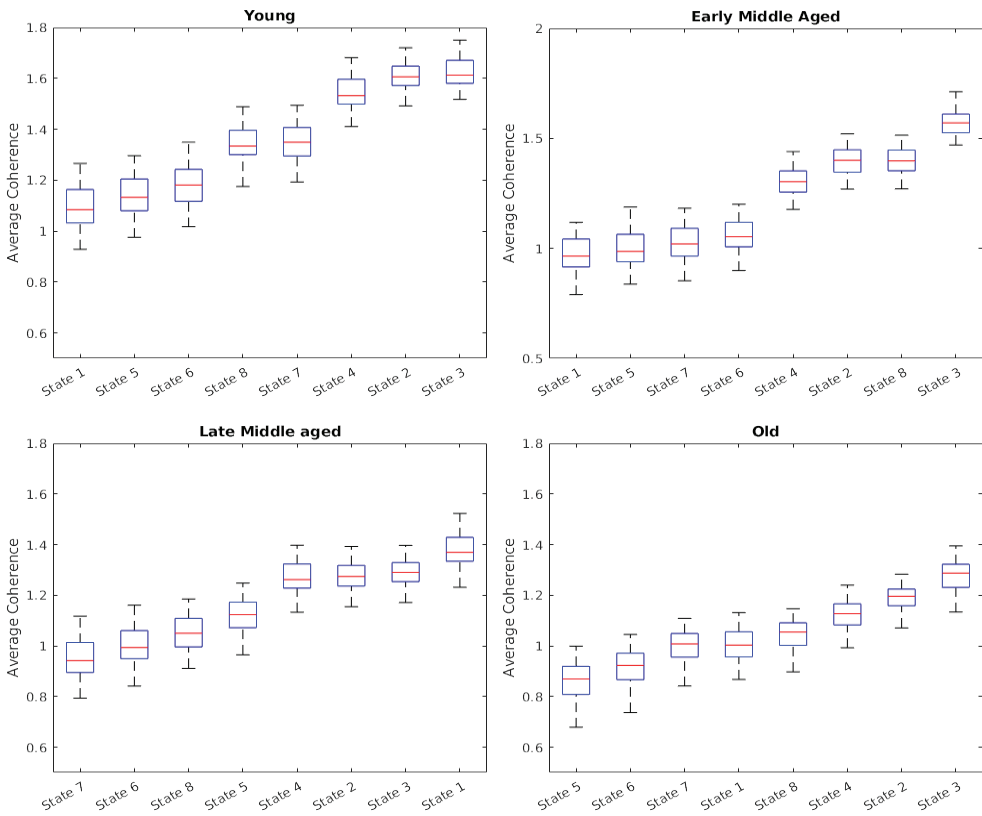


Figure 3.11: Global coherence in all states: Global coherence over all pairs of regions in the wideband frequency range, plotted in the increasing order of mean coherence for all age groups. Mean coherence for each state is marked in red.

Figure 3.11 shows increased global coherence in State 3 followed by State 2, State 4 in the wideband frequency range. The sequence of states showing low to high values is different in all age groups. The absolute values can also be seen to consistently decrease as we go from the young age group to the older age groups. Two-way ANOVA yielded significant main effect of age ($F(3, 2175) = 2070.9, p < 0.001$) as well as states ($F(7, 2175) = 1599.6, p < 0.001$). Additionally, the interaction effect between the two measures of comparisons was also found to be significant ($F(21, 2175) = 222.61$,

$p < 0.001$). The overall mean global coherence was larger in State 3 ($M = 1.44$) and least in State 5 ($M = 1.03$). In the wideband thresholded spectra, the young group had an overall higher global coherence ($M = 1.36$, $SD = 0.002$). Post-Hoc Bonferroni correction further showed significant differences in the global coherence between all age groups ($p < 0.001$).

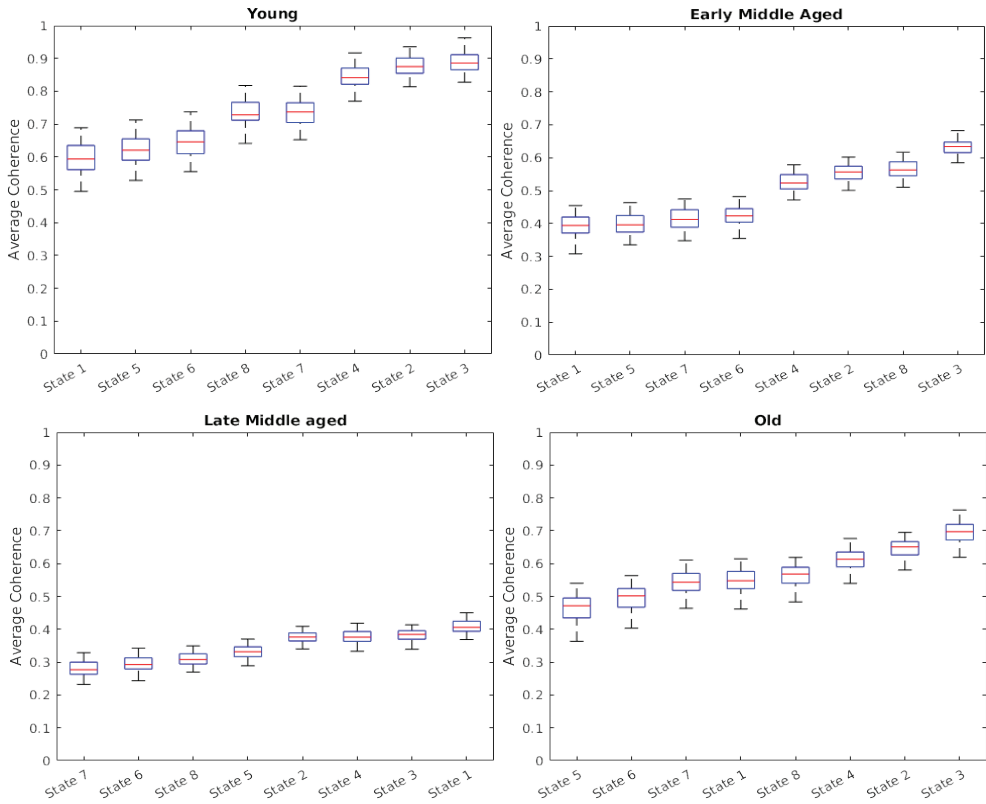


Figure 3.12: Global coherence in all states in the theta frequency range: Global coherence over all pairs of regions in the theta band frequency range plotted in the increasing order of mean coherence for all age groups. Mean coherence for each state is marked in red.

The decrease in absolute coherence values is also noticeable in the theta band thresholded frequency range. The sequence of the states is again different in all age groups, however, it matches the sequence in wideband ranges in a specific age group. This suggests that resting-state global coherence between regions in a particular state reorganizes in a manner to keep the coherence relatively constant as a person grows older. From figures 3.12 and 3.13, we can see a reverse pattern of global coherence in

theta and alpha frequency ranges. The coherence in the theta range is high in the young group and gradually decreases with age and again increases in the old group. Statistical testing using two-way ANOVA revealed significant main effects of age ($F(3, 2175) = 1653.3, p < 0.001$) and state ($F(7, 2175) = 1640.1, p < 0.001$) in the theta band global coherence. The interaction term was also found to be statistically significant ($F(21, 2175) = 214.22, p < 0.001$). The mean global coherence was highest in the case of State 3 ($M = 0.65$) and least in State 5 ($M = 0.45$), just like the wideband condition. However, in the theta band, the young group was found to have the largest ($M = 0.74, SD = 0.001$) mean global coherence. The lowest mean coherence was seen in the case of the late middle-aged group ($M = 0.34, SD = 0.001$).

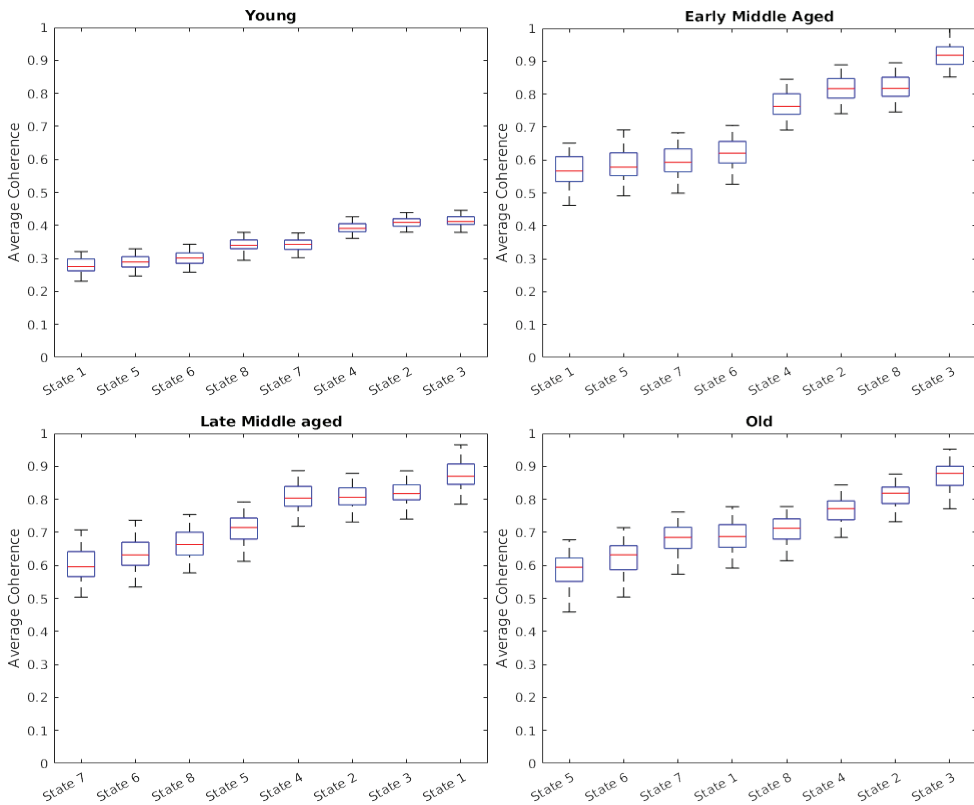


Figure 3.13: Global coherence in all states in the alpha frequency range: Global coherence over all pairs of regions in the alpha band frequency range plotted in the increasing order of mean coherence for all age groups. Mean coherence for each state is marked in red.

In the alpha band (Figure 3.13), the coherence can be seen to be relatively lower

in the young group, increases with age and then decreases in the old group. Again, there were significant main effects of age ($F(3, 2175) = 2866.2, p < 0.001$), states ($F(7, 2175) = 1323.9, p < 0.001$) and a significant interaction term ($F(21, 2175) = 320.24, p < 0.001$). However, one major difference seen in the alpha band compared to the theta band was that the largest mean global coherence was found in the late middle-aged group ($M = 0.74, SD = 0.0013$) and the least in the old group ($M = 0.32, SD = 0.0013$). State 3 ($M = 0.63$) and state 6 ($M = 0.45$) were found to have the largest and the smallest mean coherence, respectively. Figure 3.14 shows the same sequence of states in particular age groups, and a non-linear trend of change in global coherence values with significant main effects of age ($F(3, 2175) = 2253.9, p < 0.001$) and state ($F(7, 2175) = 1277.3, p < 0.001$). The effect of the interaction term was also significant in this case ($F(21, 2175) = 203.48, p < 0.001$). Similar to the alpha band thresholded spectra, State 3 showed the largest mean coherence ($M = 0.69$) and State 6 showed the least mean coherence ($M = 0.51$) compared to other states. The early middle-aged group also showed the lowest mean coherence ($M = 0.27$) in the beta band. The largest mean coherence was seen in the case of the late middle-aged group ($M = 0.74, SD = 0.0014$)

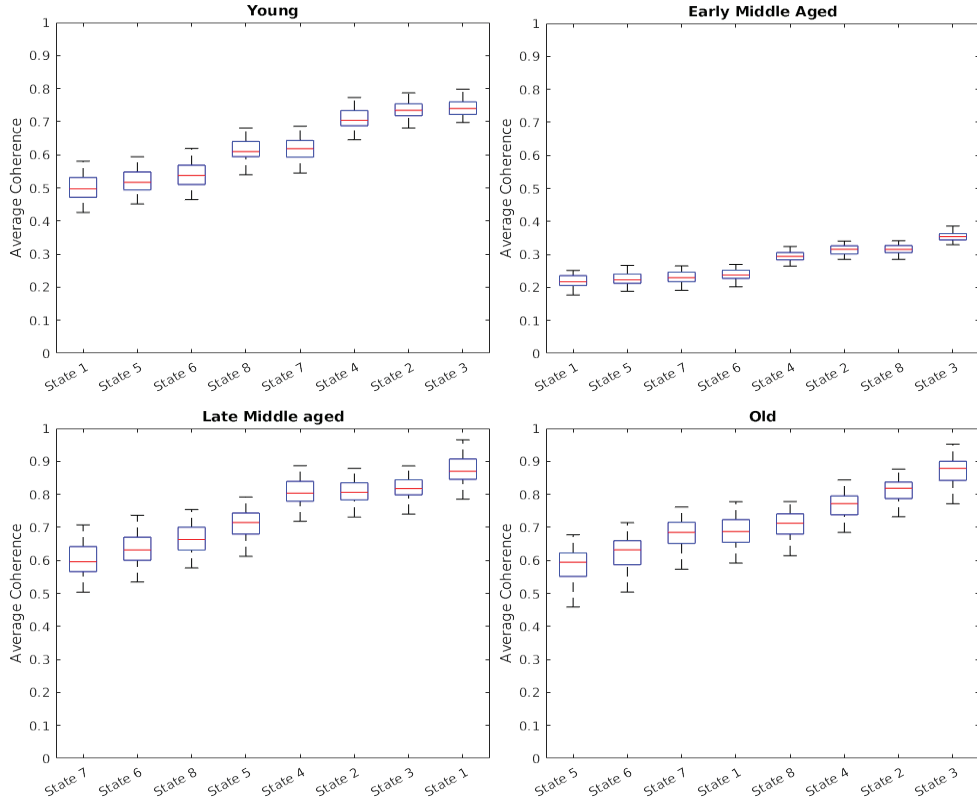


Figure 3.14: Global coherence in all states in the beta frequency range: Global coherence over all pairs of regions in the beta band frequency range plotted in the increasing order of mean coherence for all age groups. Mean coherence for each state is marked in red.

3.3.2 Global coherence in theta and alpha bands show inverse age-related trends

We wanted to see how the global coherence in a particular state changes with age in each frequency range. All states except State 1 showed a generally decreasing trend with age in the wideband condition (Figure 3.15). In the theta frequency range, all states showed a U-shaped global coherence change with age. The maximum global coherence in the young group gradually decreases in the early and late middle-aged groups and again increases in the old group (Figure 3.16). This consistent pattern could give us important insights into the compensation hypothesis of aging, which suggests an increase in theta band power in response to a related decrease in alpha band

power as a person gets older. Two-way ANOVA and subsequent correction for multiple comparisons showed that the differences between the coherence measures of each state compared across age groups were highly significant ($p < 0.001$) for all frequency bands. A significant main effect of frequency was also found in all states when compared along age groups ($p < 0.001$). The mean coherence was found to be higher in the beta band for all states ($0.51 < M < 0.69$). The pattern of change in global coherence in the alpha band indeed showed an upside-down U-shaped trend with age (Figure 3.17). This suggests that frequency plays an essential role in reorganizing transient brain networks to compensate for the dynamical changes associated with healthy aging. A non-linear trend of change in global coherence was seen in the case of beta band thresholded spectra (Figure 3.18). Previous studies had not seen any correlation between global coherence in the beta band with age. However, the consistent pattern of coherence in all states reveal a decrease in whole-brain coherence in the early middle-age, followed by a sharp increase. This could be indicative of a generalized increase in modularity or non-specific connections between brain regions, to prevent loss of overall cognitive power. Previous studies have found a decrease in motor performance with increased beta power in older adults. However, the increased power was not predictive of motor performance [62].

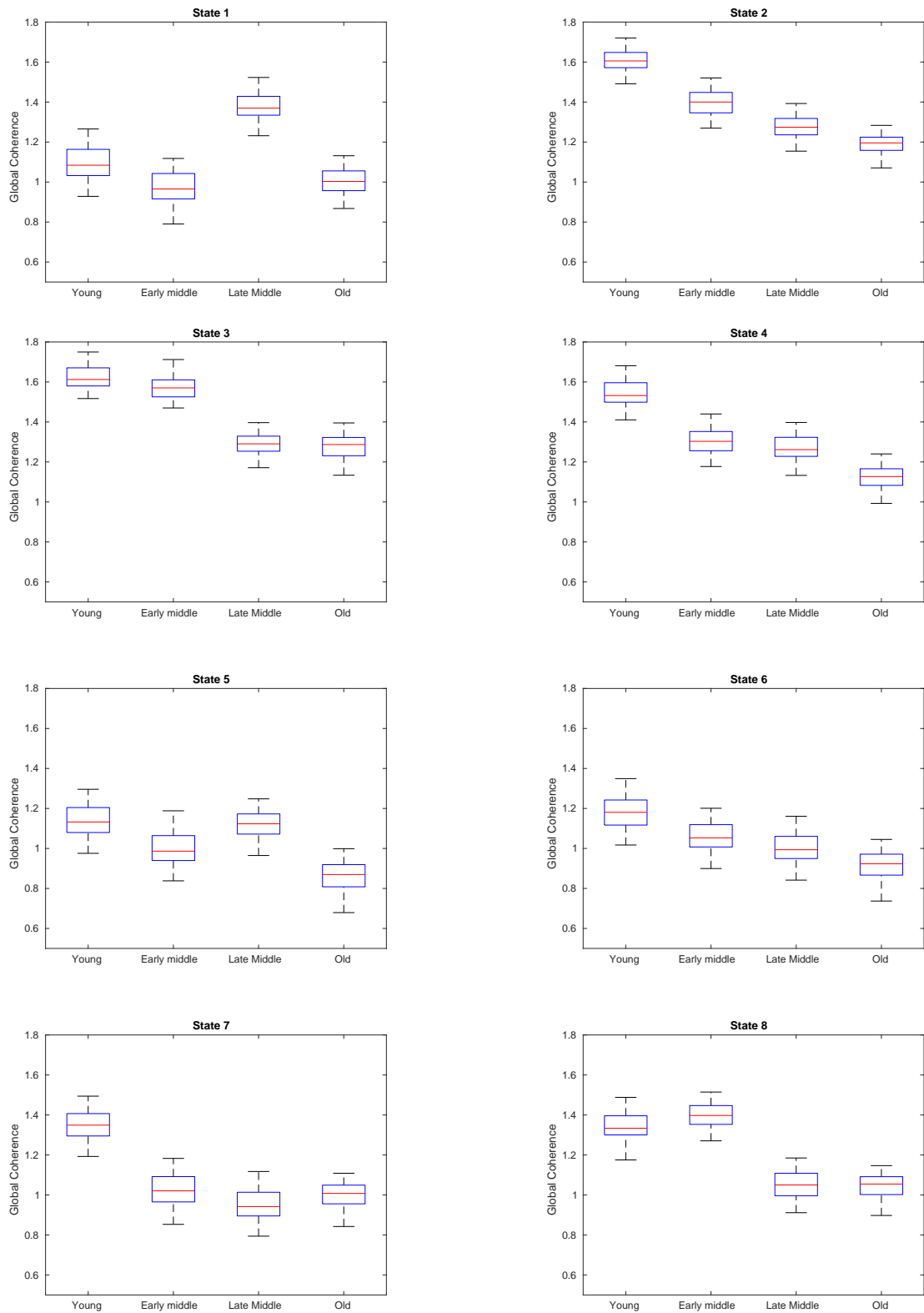


Figure 3.15: Comparison of change in coherence in the wideband frequency range for each state across all age groups. The box plots show the mean and distribution of the global coherence in the wideband thresholded power spectra. Mean coherence for each age group is marked in red.

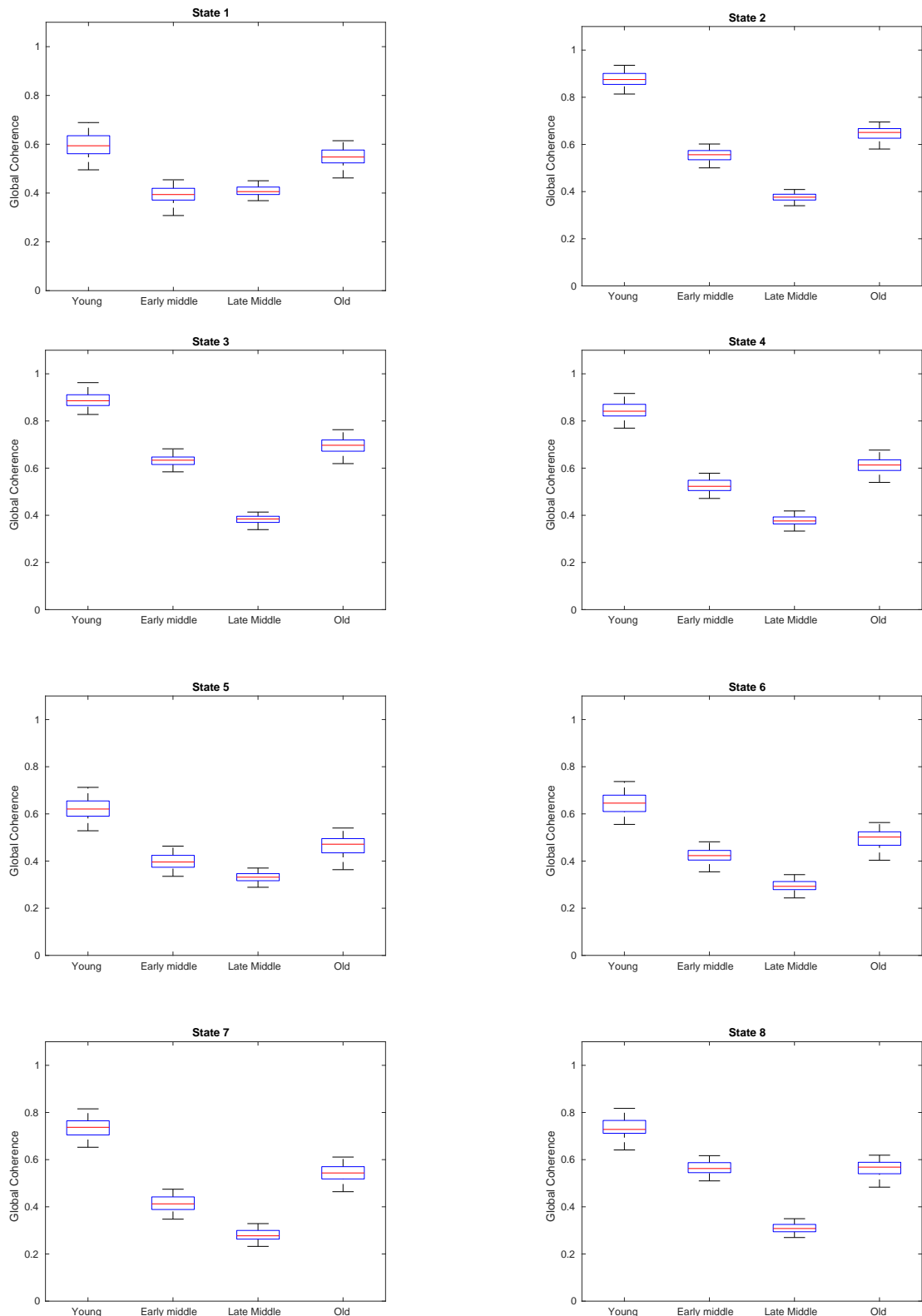


Figure 3.16: Comparison of change in coherence in the theta band (0.5-10 Hz) frequency range for each state across all age groups. The box plots show the mean and distribution of the global coherence in the theta band thresholded power spectra. Mean coherence for each age group is marked in red.

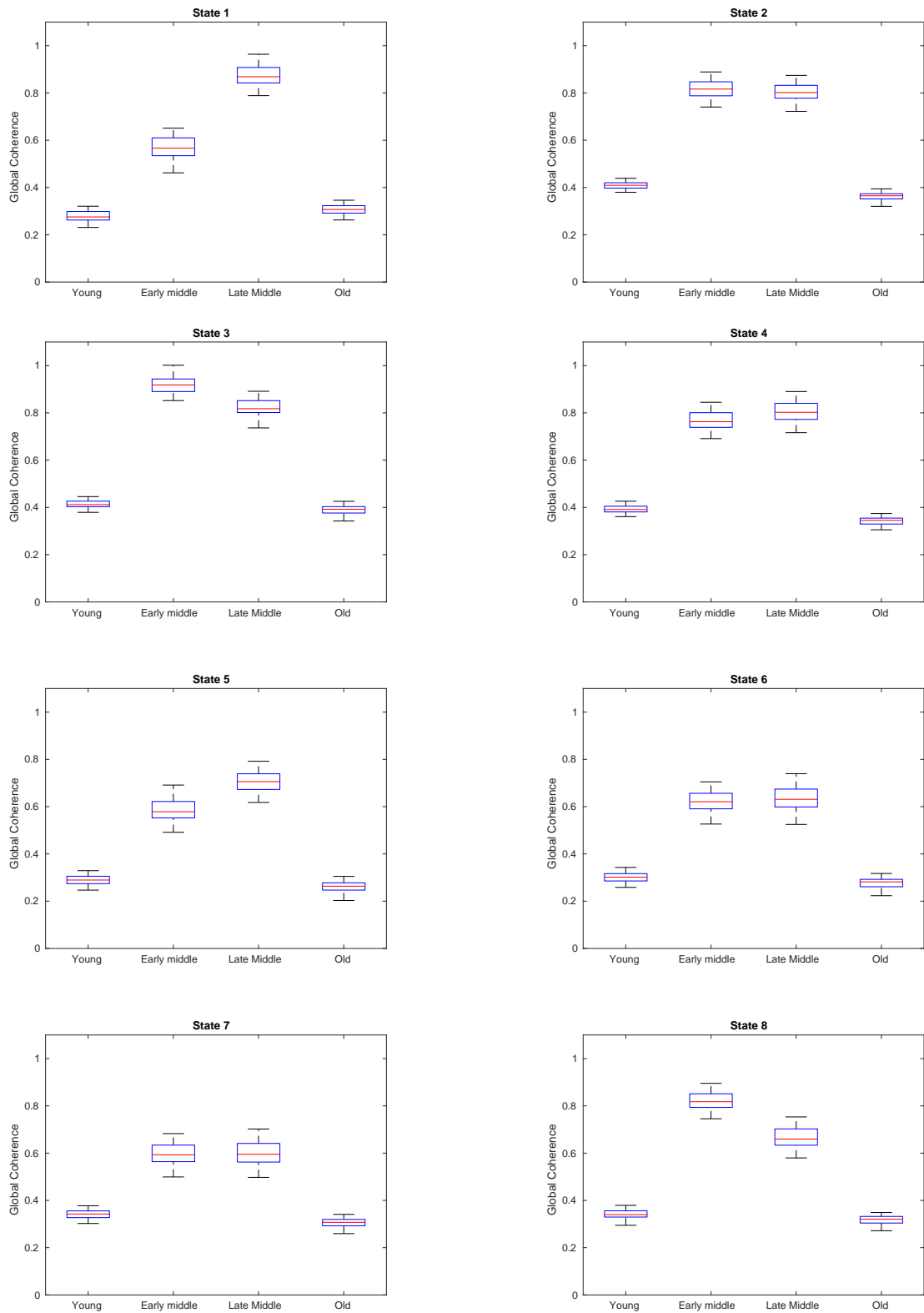


Figure 3.17: Comparison of change in coherence in the alpha band (5-15 Hz) frequency range for each state across all age groups. The box plots show the mean and distribution of the global coherence in the alpha band thresholded power spectra. Mean coherence for each age group is marked in red.

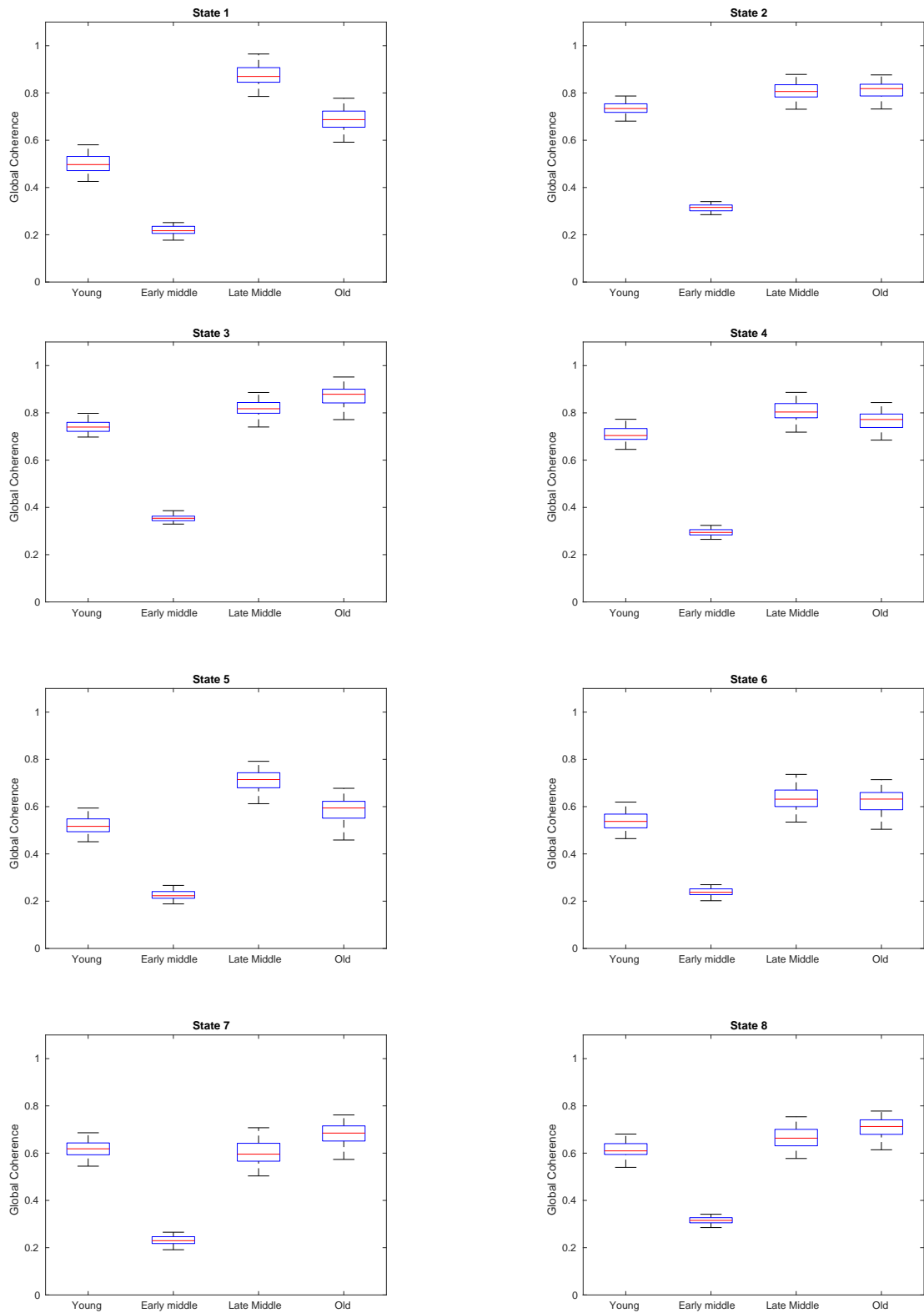


Figure 3.18: Comparison of change in coherence in the beta band (15-30 Hz) frequency range for each state across all age groups. The box plots show the mean and distribution of the global coherence in the beta band thresholded power spectra. Mean coherence for each age group is marked in red.

3.4 Network Connectivity

3.4.1 Phase based connectivity in the brain does not show dynamic changes with age

An important question to consider was whether the coherence connectivity is driven only by the power or if there is a significant contribution of phase coupling also that drives the connectivity between brain regions in particular transient states. We wanted to investigate which measure was more significant in driving the age-related connectivity changes between the brain regions and focus our analysis on the theta and alpha bands because of their implication in aging, as suggested by previous studies. We used phase lag index (PLI) to check for phase connectivity and synchronization between two brain regions. Interestingly, when the whole brain phase lag index in all states are compared across age groups, it shows a different pattern than coherence (Figure 3.19 and Figure 3.20). The highest PLI value was found in State 5 ($M = 0.005$) and the early middle-aged group ($M = 0.003$) in the theta band. In the alpha band, State 5 again showed a larger mean PLI ($M = 0.007$) along with an overall higher mean in the late middle-aged group ($M = 0.0036$).

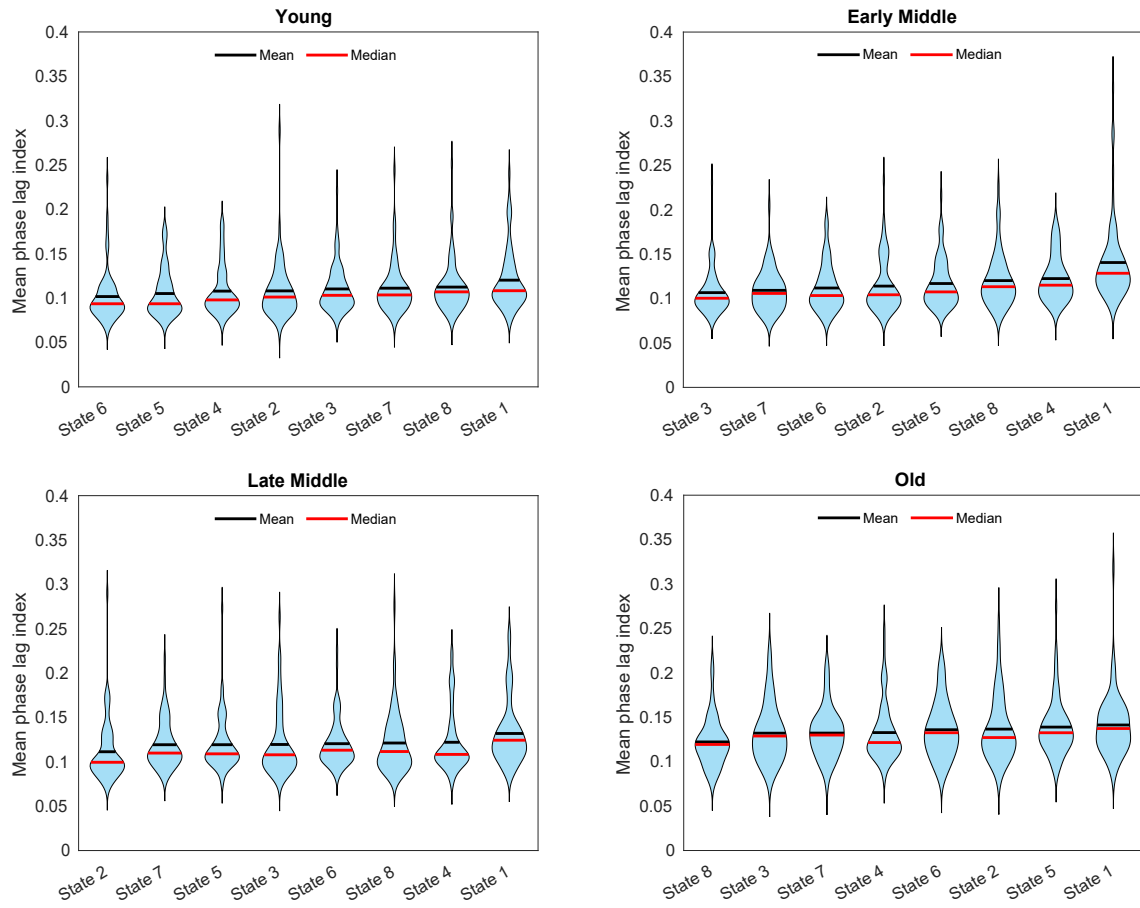


Figure 3.19: Phase lag index: Comparison of strength of phase coupling in each state in the theta frequency range along each age group. Mean phase lag index for each state is arranged in ascending order for all ages.

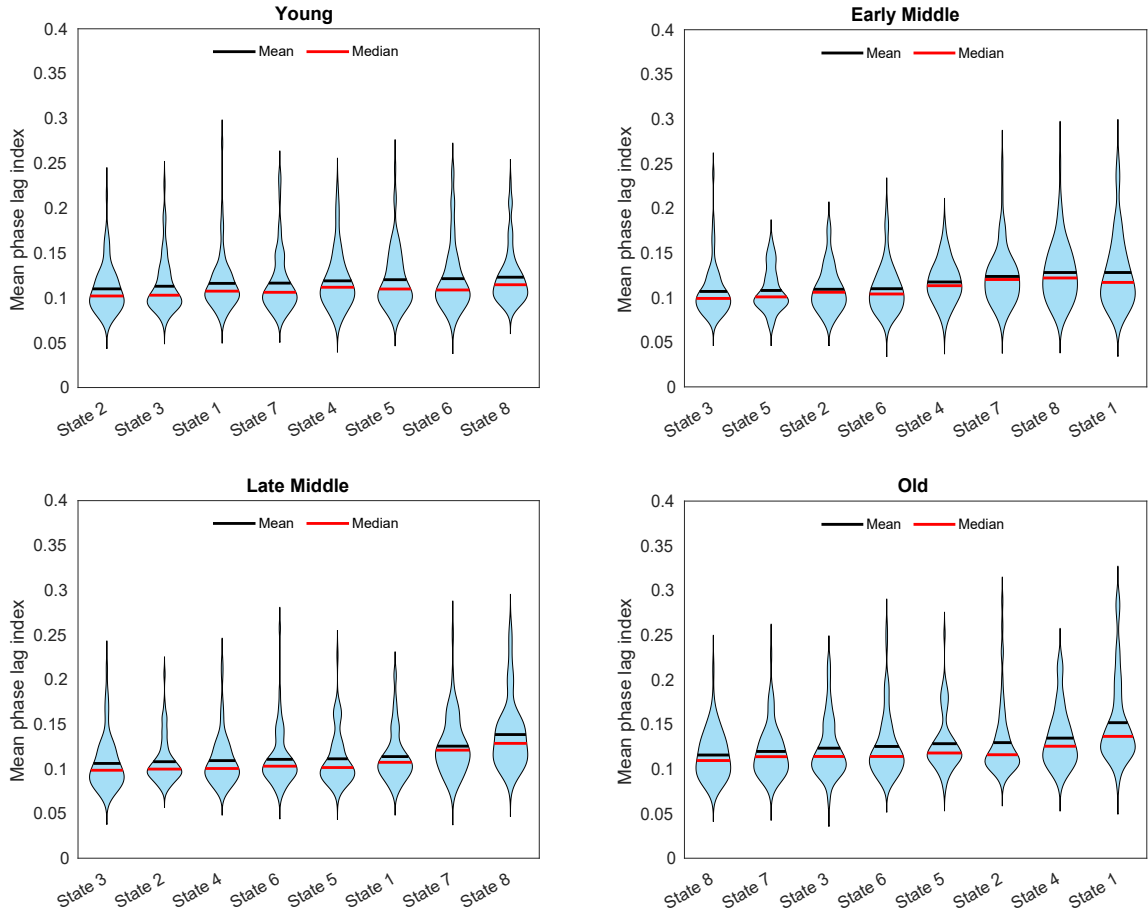


Figure 3.20: Phase lag index: Comparison of strength of phase coupling in each state in the alpha frequency range along each age group. Mean phase lag index for each state is arranged in ascending order for all ages.

PLI of brain regions thresholded in theta and alpha narrowband ranges show different patterns. We performed two-way ANOVA to quantify PLI changes with age and state as the main factors. We found a significant main effect of states on the PLI values, but the main effect of age was found to be insignificant in the 95% confidence interval in both theta ($F(3, 2175) = 2.38, p = 0.06$) and alpha ($F(3, 2175) = 0.31, p = 0.81$) frequency ranges. Post-Hoc Tukey's test did not reveal any significant changes in PLI values with age ($p > 0.1$). Additionally, the interaction effect also did not reach statistical significance in both bands ($p = 0.89$ and $p = 0.74$). See Tables 5.4 and 5.5 for all the summary statistics between PLI measures of different age groups.

3.4.2 Connectivity analysis in specific parcels of power activation

Cluster-based statistical testing was employed to understand the change in coherence in specific networks with age and frequency. Clusters of brain regions commonly activated in all age groups in particular frequency bands were selected for further analysis. Volumetric brain maps were generated with the power spectral density in each state and a particular frequency band to show activation in the brain space. These maps showed similar activation across ages, and the common parcels were identified. The coherence values corresponding to these parcels were studied to see how the connectivity pattern changes with age and frequency. Thus, coherence was seen to drive connectivity changes across age, both globally and in particular parcels of interest. In contrast, phase-based connectivity was only found to drive global connectivity changes and not in specific clusters. In each state, the thresholded PLI values between the cluster nodes were not found to be statistically significant after multiple corrections (see Table 5.7 for comparisons between cluster based PLI values between all age groups). Thus, we decided to compare the connectivity among age groups in terms of coherence (See Table 5.6 for comparisons between cluster based coherence values between all age groups). Two-way ANOVA was performed in a 4×8 factorial design with age and states as the main factors to check if the cluster-based coherence showed significant variability with age. Main effects of age ($F(3, 2175) = 47.49, p < 0.001$ and $F(3, 2175) = 99.53, p < 0.001$, respectively) and state ($F(3, 2175) = 15.83, p < 0.001$ and $F(3, 2175) = 46.14, p < 0.001$, respectively) for both theta and alpha bands were found to be significant.

The circular connectivity plots show the connections between two brain regions (indicated by the nodes, which signify parcel numbers or brain regions). Figures 3.21-3.28 show the side-by-side connectivity plots in theta and alpha band thresholded spectra, based on coherence between two nodes in a cluster. The coherence values are thresholded to show the 50% strongest connections.

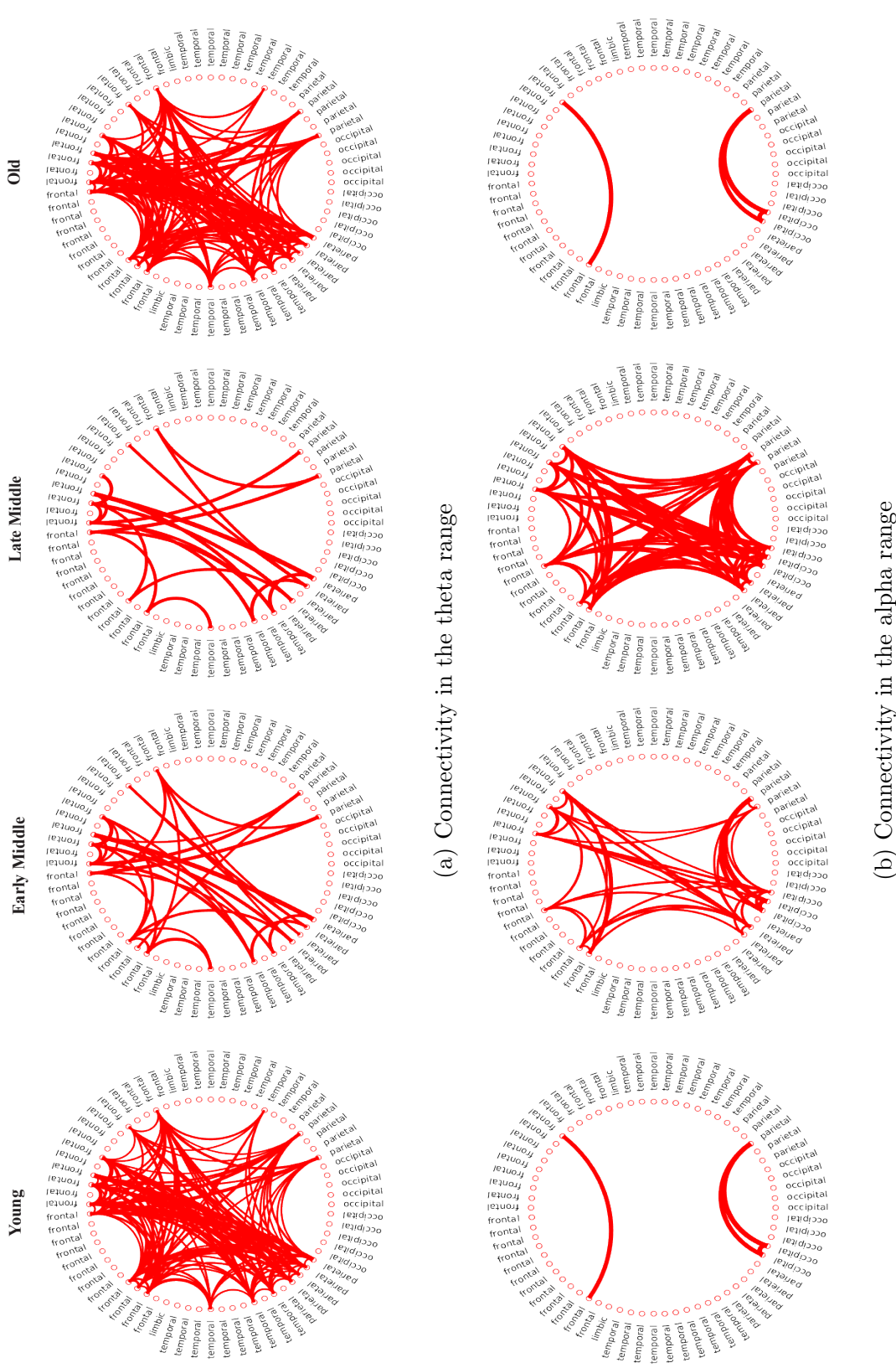


Figure 3.21: Spectral connectivity: Comparing the 50% strongest connections across age in the a) theta and b) alpha frequency bands in State 1. The nodes indicate the lobes to which the parcels (frontal, limbic, temporal, parietal and occipital). From left to right, connectivity patterns are shown for: Young, Early Middle, Late Middle and Old age groups.

From Fig. 3.21a, we can see that in the young group, there are many connections between bilateral rostral and caudal middle frontal regions, bilateral superior frontal, superior parietal and superior temporal regions. Right rostral and caudal anterior cingulate cortex and inferior parietal lobe are also coherence-based connectivity in the theta range. Parcel-wise connection strength in mostly the frontal regions survives as we go from young to early middle-ages. Almost no parietal or temporal connections survived the thresholding criteria in the late middle-aged group. Interestingly, in the old age group, the connections between bilateral inferior parietal, superior parietal and middle temporal are again seen to have significant connection strength between themselves and the frontal regions. Thus, theta band coherence and connection strength between brain regions were found to remain stable in the frontal areas and deteriorate in the posterior areas of the brain with age. The coherence based connection strength between anterior and posterior regions is again seen to increase in the old age group in the theta frequency range. In the alpha band thresholded connectivity maps shown in Fig. 3.21b, State 1 shows high connectivity in posterior regions, mainly bilateral occipital and parietal areas with some connections in the rostral middle frontal areas and right superior frontal areas in both the middle-aged groups. In young and old groups, the connectivity is lower and mainly contained in posterior regions like bilateral cuneus, precuneus, and left fusiform areas. Comparison between the connection strengths across frequency in 4×2 (age, frequency bands) revealed a significant main effect of frequency ($F(1, 543) = 10.12, p = 0.0016$) and an interaction effect ($F(3, 543) = 19.97, p < 0.001$) for State 1, with higher mean connectivity in the theta band ($M = 0.021$) than the alpha band ($M = 0.01$).

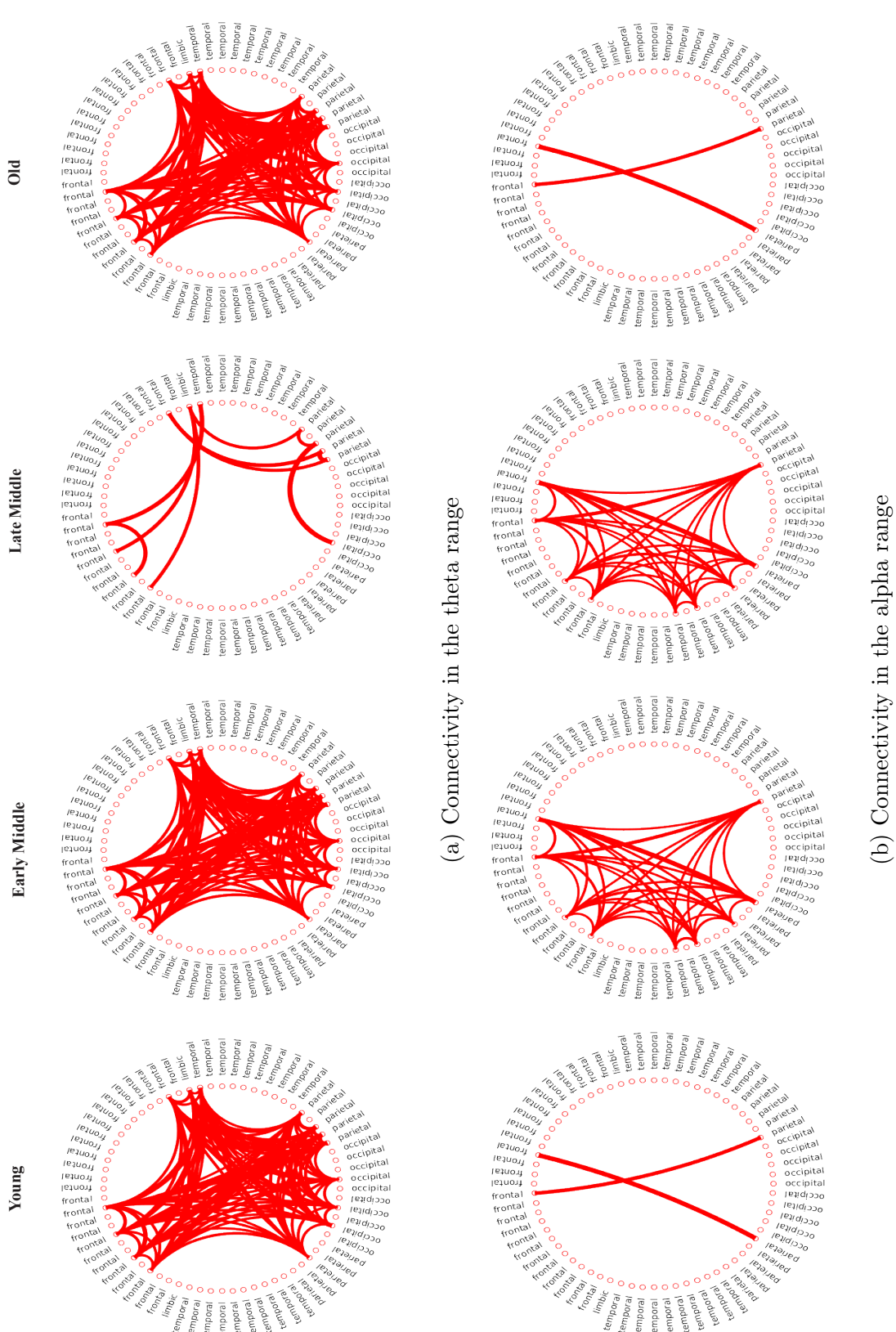


Figure 3.22: Spectral connectivity: Comparing the 50% strongest connections across age in the a) theta and b) alpha frequency bands in State 2. The nodes indicate the lobes to which the parcels (frontal, limbic, temporal, parietal and occipital). From left to right, connectivity patterns are shown for: Young, Early Middle, Late Middle and Old age groups.

In State 2 (Fig.3.22a) and State 3 (Fig. 3.22a) the young age group shows connectivity in frontal as well as parietal and temporal regions in the theta band. Connectivity in State 3 also includes connections in the right postcentral and precentral regions and left lingual and posterior cingulate cortex. State 2 shows a similar trend as State 1 across age, where only the frontal connections remain stable with age. In State 3, however, in addition to significant frontal connections, posterior connections also survive the threshold. In the old group, both states show a pattern of connectivity similar to their young counterpart. In the case of the alpha band, State 2 (see Fig.3.22b) shows high connectivity among the left inferior temporal, left inferior parietal, left middle temporal, right caudal middle frontal and superior frontal regions in both middle-aged groups. Very few connections survive the threshold between the young and old age groups, mostly between the parietal regions. In Fig.3.23b) we can see that the connectivity is generally very high, spanning bilateral lingual, bilateral anterior and posterior cingulate, left superior parietal, precuneus, precentral and paracentral regions, as well as right inferior parietal, inferior temporal, superior parietal, superior temporal, superior frontal and orbitofrontal regions. Again, this whole-brain anterior-posterior connectivity is significantly reduced in the young and old age groups, and the only connections that survive are the temporal and parietal connections. The interaction effect is significant in both States 2 and 3 ($F(3, 543) = 8.23, p < 0.001$ and $F(3, 543) = 32.4, p < 0.001$ respectively), with a higher overall mean in the alpha band ($M = 0.0068$ and 0.08 respectively).

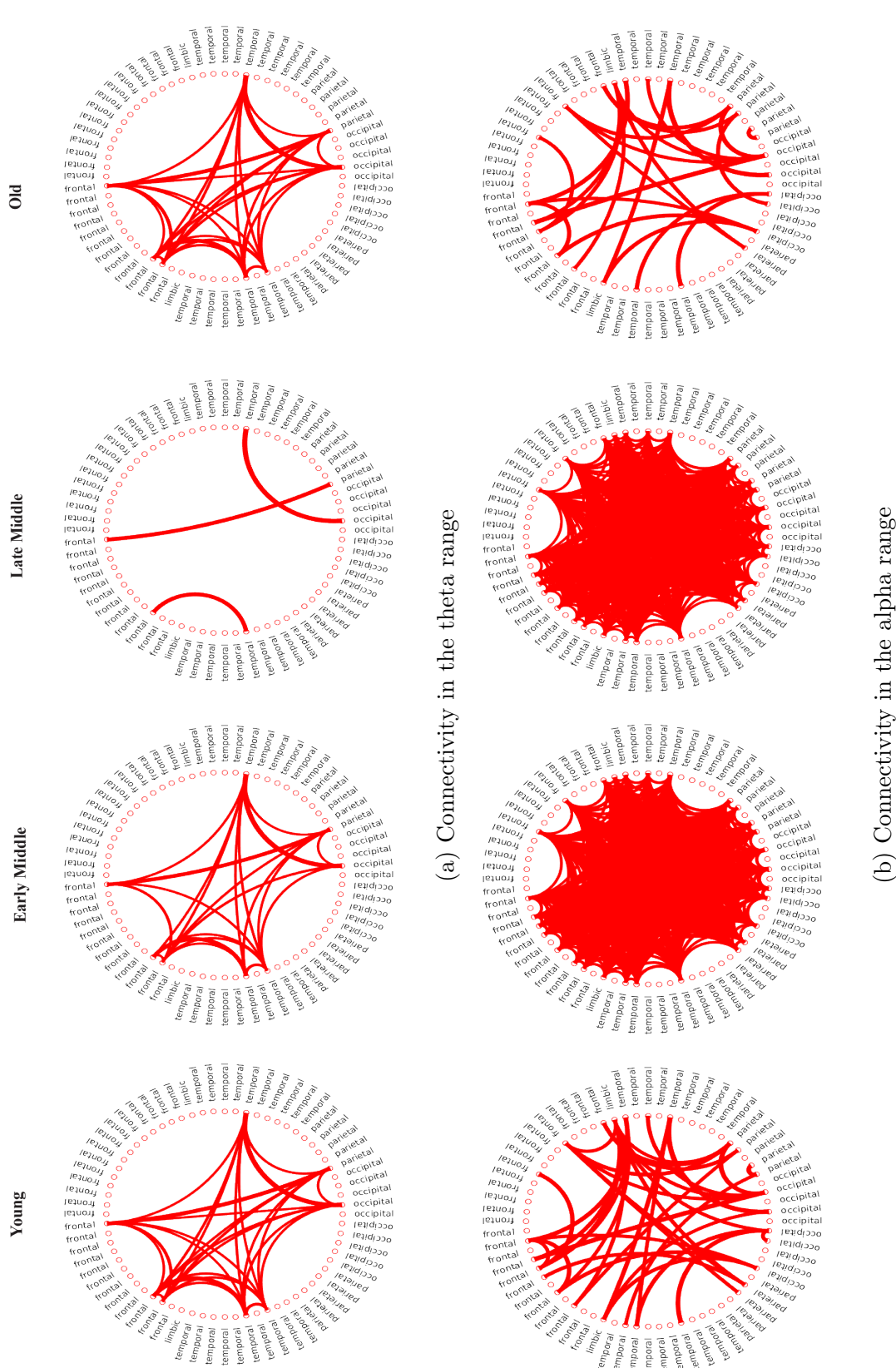


Figure 3.23: Spectral connectivity: Comparing the 50% strongest connections across age in the a) theta and b) alpha frequency bands in State 3. The nodes indicate the lobes to which the parcels (frontal, limbic, temporal, parietal and occipital). From left to right, connectivity patterns are shown for: Young, Early Middle, Late Middle and Old age groups.

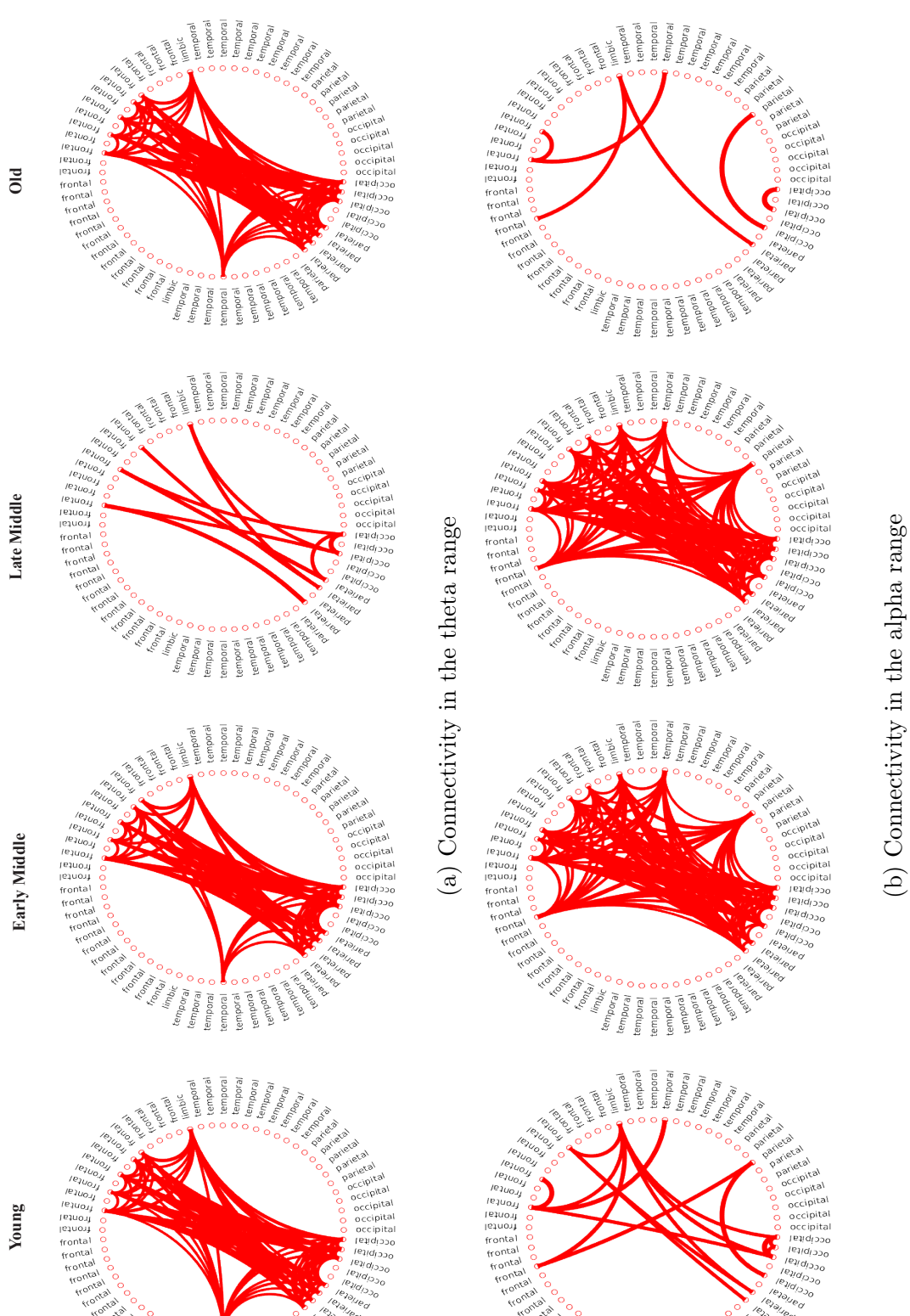


Figure 3.24: Spectral connectivity: Comparing the 50% strongest connections across age in the a) theta and b) alpha frequency bands in State 4. The nodes indicate the lobes to which the parcels (frontal, limbic, temporal, parietal and occipital). From left to right, connectivity patterns are shown for: Young, Early Middle, Late Middle and Old age groups.

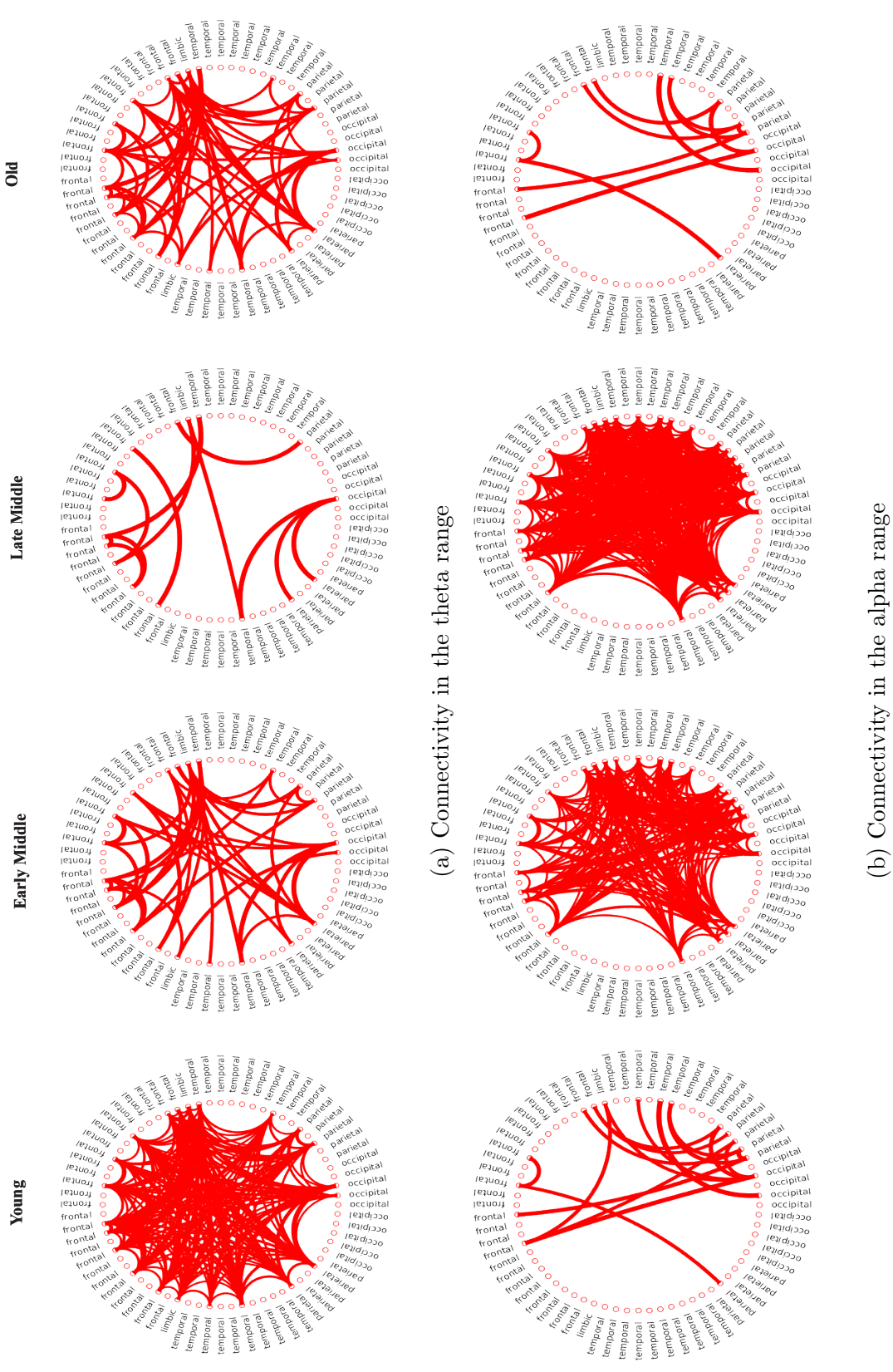


Figure 3.25: Spectral connectivity: Comparing the 50% strongest connections across age in the a) theta and b) alpha frequency bands in State 5. The nodes indicate the lobes to which the parcels (frontal, limbic, temporal, parietal and occipital). From left to right, connectivity patterns are shown for: Young, Early Middle, Late Middle and Old age groups.

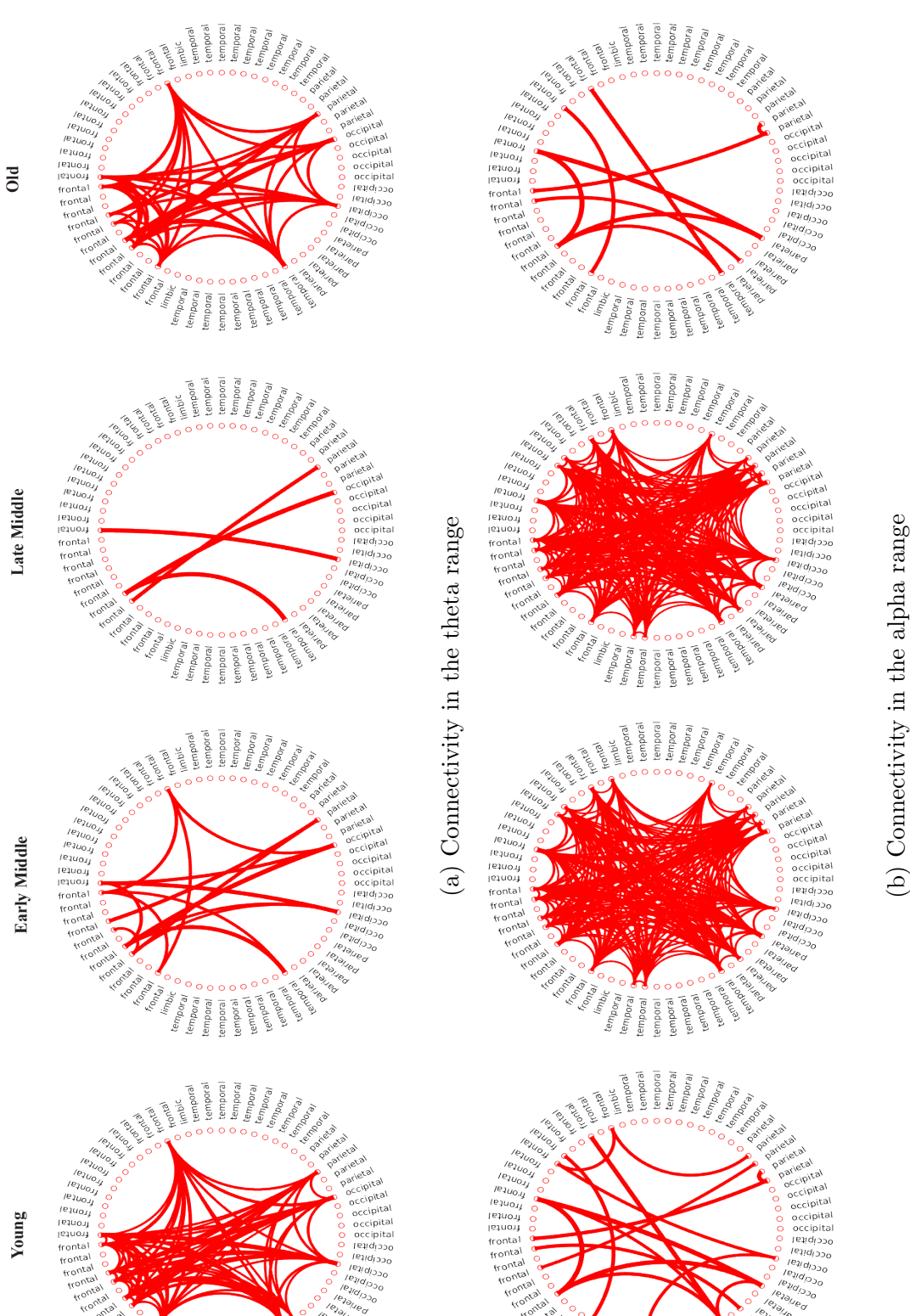


Figure 3.26: Spectral connectivity: Comparing the 50% strongest connections across age in the a) theta and b) alpha frequency bands in State 6. The nodes indicate the lobes to which the parcels (frontal, limbic, temporal, parietal and occipital). From left to right, connectivity patterns are shown for: Young, Early Middle, Late Middle and Old age groups.

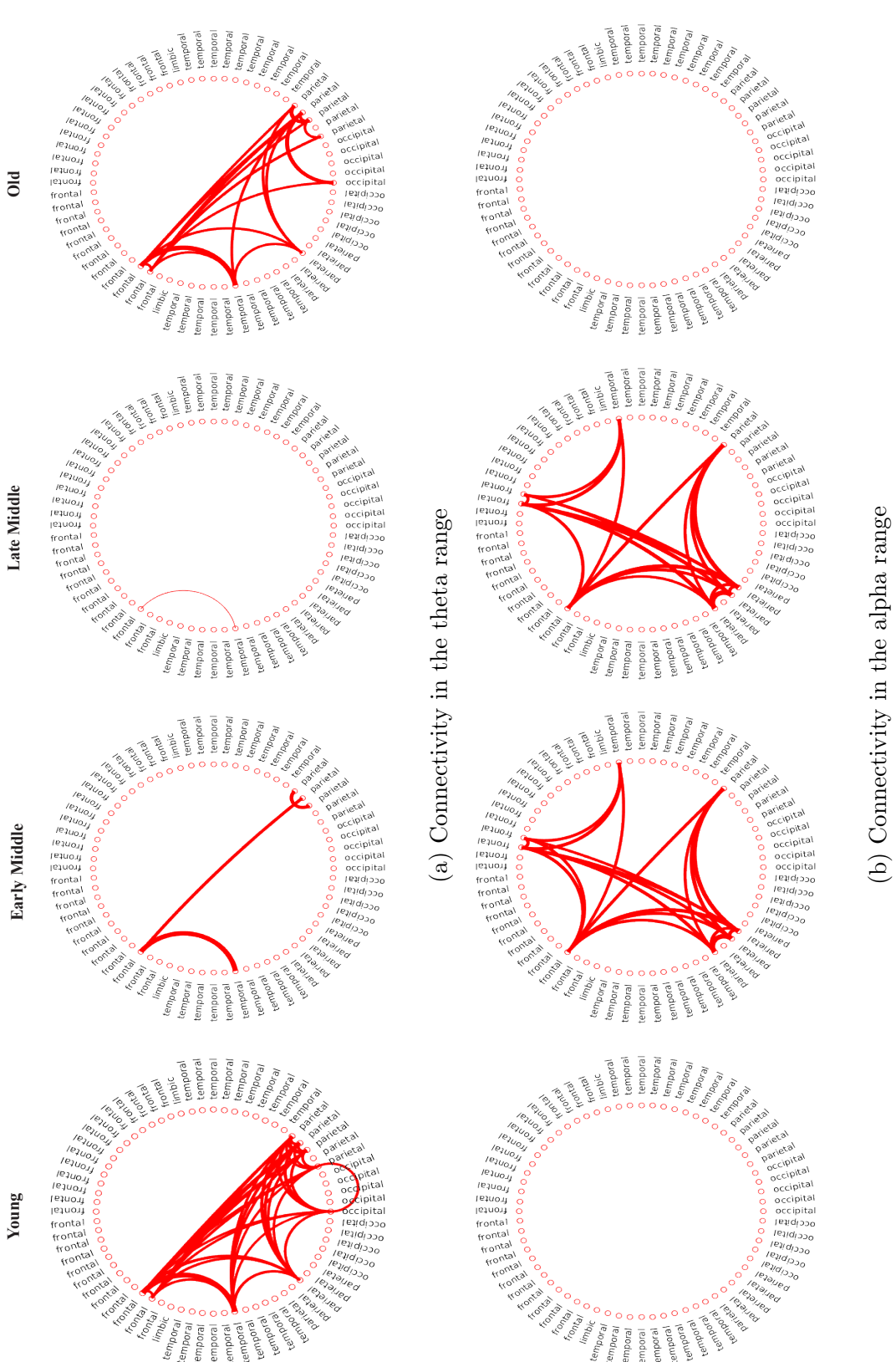


Figure 3.27: Spectral connectivity: Comparing the 50% strongest connections across age in the a) theta and b) alpha frequency bands in State 7. The nodes indicate the lobes to which the parcels (frontal, limbic, temporal, parietal and occipital). From left to right, connectivity patterns are shown for: Young, Early Middle, Late Middle and Old age groups.

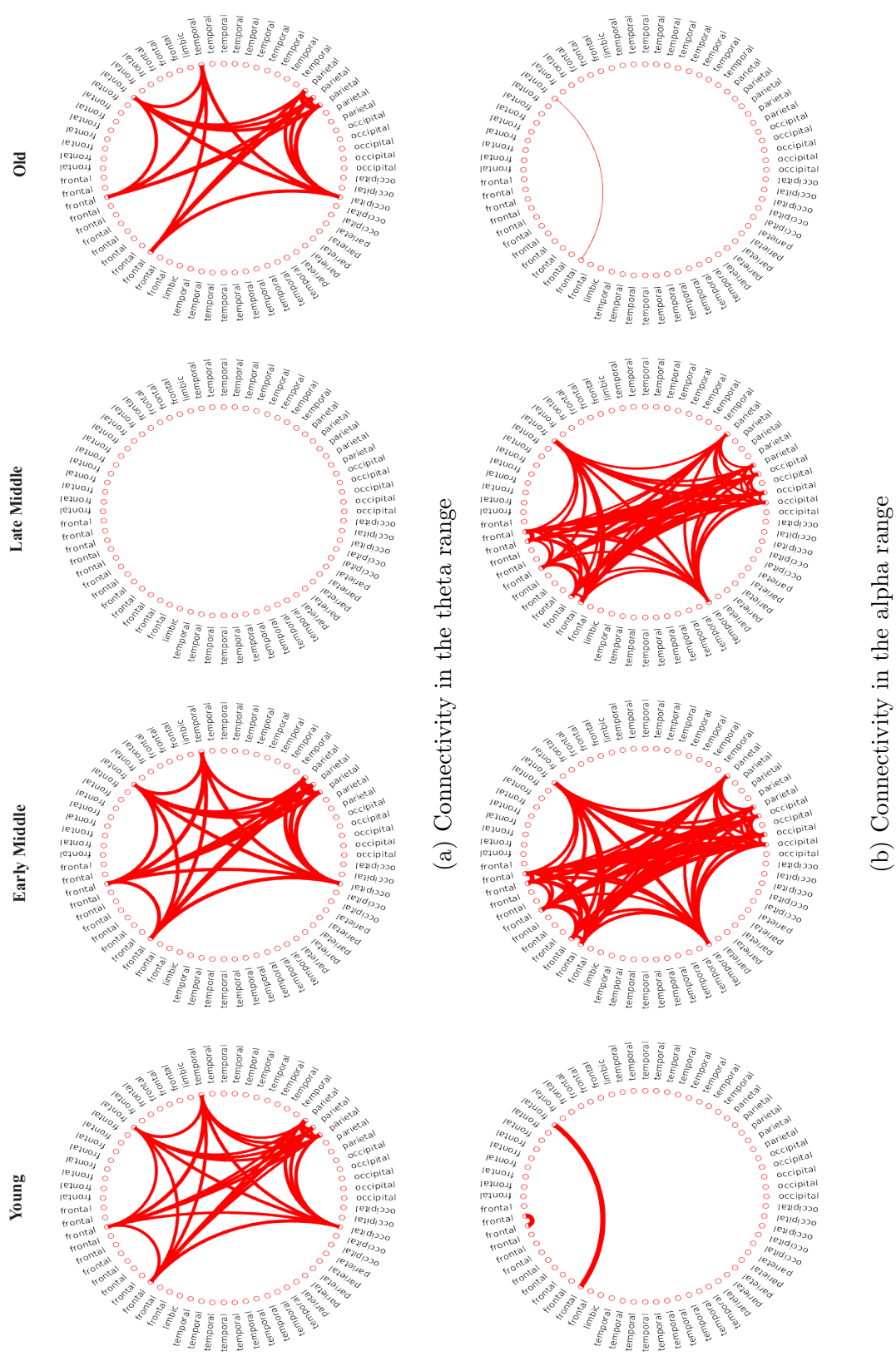


Figure 3.28: Spectral connectivity: Comparing the 50% strongest connections across age in the a) theta and b) alpha frequency bands in State 8. The nodes indicate the lobes to which the parcels (frontal, limbic, temporal, parietal and occipital). From left to right, connectivity patterns are shown for: Young, Early Middle, Late Middle and Old age groups.

The mean connection strength is found to be higher in the theta band for States 1, 7 and 8 ($M = 0.014$), and in the alpha band for all the other states ($M = 0.021$).

This connectivity pattern is maintained in all states, where the young and old age groups have significantly reduced connectivity between the posterior and anterior regions in the alpha range and middle-aged groups in the theta range. The previous results show the inverse behavior of alpha and theta coherence with age. We now see that the connectivity pattern between brain regions in these frequency bands also follows an inverse relationship. This further supports the hypothesis that brain networks reorganize themselves in specific frequency bands and compensate each other to maintain cognitive performance in the face of aging. High theta band connectivity between anterior and posterior regions in all states in young and old age groups may help compensate for the lower connectivity in these age groups in the alpha band. On the other hand, the higher connectivity between anterior and posterior regions in the alpha band in the middle-aged groups helps maintain overall cognitive performance.

Another interesting phenomenon observed is that the only connections between clusters that survive thresholding are the connections between posterior regions in the alpha range and the anterior connections in the theta range. The overall lowered connectivity in the theta band in early and late middle-aged groups still showed some connectivity in the anterior regions. Again, the reduced connectivity in the young and old age groups preserved the posterior connections in the alpha band. This also suggests that the reorganization of the underlying brain networks ensures that whole-brain connectivity remains unaltered in the face of aging, and the dominant frequency plays a vital role in such reorganization.

Chapter 4

Discussion

In this study, we used the Hidden Markov Model (HMM) to investigate the dynamics between large scale resting-state brain networks and their alteration with age. There were four age groups considered - Young (18-34 years), Early Middle aged (35-49 years), Late Middle aged (50-64 years), and Old (65-88 years). The HMM algorithm helps characterize recurrent patterns of spatial activation that repeat in time in an entirely data-driven manner. We used the model on source-reconstructed MEG data from 200 participants to quantify the temporal and spectral changes observed in these transient networks with age. The main findings of this investigation are as follows:

1. Eight transient states inferred from the source reconstructed MEG data resembled higher-order brain networks, visual networks and sensorimotor networks. However, not all states were found to have an exact match in their spatial activation pattern as previously established fMRI resting-state networks. This might be due to limited data points considered in the analysis (only one minute of recording was used), which led to only a few networks showing dynamically recurrent behavior with time. Another possibility is that the activity of the underlying networks is not explained by just one state but by a combination of states in time. In a study by Viduarre et al. (2018), it was seen that two different states were describing the anterior and posterior areas of the default mode network separately [53]. Further, another study by the same group used fMRI data to reveal that states might be hierarchically organized into two metastates which describe higher-order cognition and sensory and motor networks [54].

2. The spatial activation pattern showed similarities across all age groups; however, the absolute mean activation showed some age-related differences. Activation in State 1 was overall higher for all age groups except the late middle-aged group. The states themselves showed different patterns of activation values in specific clusters when compared across ages. While the trend was non-linear in most states, State 1 showed a decreasing trend, and State 3 showed an increasing trend with age. Our findings highlighted that the mean activation quantified from functional connectivity over all states does indeed decrease with age. This is in accordance with previous studies which investigated the relationship between functional connectivity and age [41]. Moreover, within network (or here, within state) functional connectivity also shows interesting patterns with age. The increasing-decreasing activation dynamics within each state could also suggest the adaptive crosstalk between the underlying functional brain networks to alleviate the effects of age-related decline.
3. We compared the temporal characteristics of the inferred HMM states between age groups to quantify the changes caused due to advancing age. The variability in the temporal characteristics gives us an interpretation of the underlying network dynamics of the dominant state at each point in time. Our analysis of the temporal characteristics yielded the following results:
 - (a) The transition probability of switching from one given state to another state at the next time point gives us an idea of cross-network interactions in the brain. A high transition probability suggests that some networks are more likely to follow others in time. Since HMM states are mutually exclusive, but the time courses are probabilistic, we can also get an idea of the temporal overlap or co-activation of these networks. This can also tell us if certain networks show an antagonism that would be evident from the low transition probabilities between them. Baker et al. (2014) [51] found a very low transition probability between DMN and DAN networks which are known to rarely co-activate, and one network must be suppressed for the other to get activated. We did not find age-related differences in the transition probabilities between states. The tendency of all states to make a switch to State 6 was found to be higher in all age groups. State 6, which resembled DMN, the brain's default state, has been shown to be the dominant network in the resting brain. Thus, the higher probability of the brain transitioning from all networks to the DMN network makes neurophysiological sense.

- (b) Fractional occupancy is another temporal measure which can provide an insight into the cross-network dynamics between transient brain states. The correlation between fractional occupancies of two states shows us how likely will two states activate together. In all age groups, States 1 and 3 and States 2 and 8 are seen to be more likely to activate simultaneously. However, if we compare each state's fractional occupancy with its counterpart in other age groups, we find a significant effect of the interaction between age and states, which is difficult to interpret directly. A change in the total time in a trial during which a state remains active could ultimately lead to a change in co-activation between states, which suggests a weakening of functional connectivity between brain regions.
 - (c) Differences between state switching rates and mean lifetimes of each state across ages give us important information about the temporal stability of the states. State 3, for example, is not found to be active for more than 50ms at a time in most age groups, leading to higher instability than any other state. The spatial map of State 3 suggested that it might describe a visual network, which can be explained to show more random activations and instability in the eyes-closed state. A decrease in the state's lifetime could be interpreted as more fluctuations or faster transitions between states as a person grows older. Vidaurre et al. [54] showed that the time spent visiting each state and the time during which a state remains active is not random and could be acting as a preparatory stage for the incoming task. The shift in these measures with healthy aging could also provide a deactivation basis for reducing cognitive performance, i.e. with age, the increase or decrease in mean lifetimes of a particular transient state may inhibit the deactivation of resting networks efficiently which leads to poor task performance. These four measures together constitute the ‘structural chronnectome’ of each state.
4. Change in global coherence with age in major frequency bands showed interesting and consistent patterns in all states. An overall decreasing trend in global coherence was seen in the wideband (0-40 Hz) frequency spectra in most states. The reduction in whole-brain global coherence may be attributed to altered excitation-inhibition balance between local brain areas due to age-related decline in tissue properties. Another possible explanation behind this reduction might be cred-

ited to an increase in neural noise in the older individuals, which brings down the whole-brain coherence [63]. Theta (0.5-10 Hz) and alpha (5-15 Hz) band thresholded spectra showed opposite trends of change in global coherence with age. In the theta band, all states showed a U-shaped pattern of change in global coherence as we went from younger to older age groups. In the alpha band, this trend was reversed, and an inverse U-shaped pattern was found. This suggested that a compensation mechanism might be at play which prevents the reduction of overall coherence between brain regions by dynamically reorganizing the spectral properties of whole-brain networks. Global coherence in the beta band thresholded spectra was seen to follow a non-linear trend, with higher coherence in the young age group followed by a drop in the early middle-aged group. It increases again in the late middle-aged group and remains relatively similar in the older group.

5. Connectivity between brain regions in different transient states was also seen to be affected by phase coupling in previous studies[53]. The phase lag index used to quantify the phase coupling between two brain regions followed a different trend with age than coherence. However, in specific spatial clusters of power (higher than the global average) in each state, the PLI measures in specific frequency bands did not show any significant differences with age. Coherence based connectivity between regions in the significant clusters revealed another interesting phenomenon. Reduced connectivity was found in all states in the middle-aged groups in the theta and the young and old groups in the alpha band. The higher connectivity in both cases was found to span both anterior and posterior regions. The reduction was more severe for posterior connections in the theta band and anterior connections in the alpha band. This further supports the hypothesis of a compensatory mechanism in the reorganization of transient brain networks, allowing dynamic cross-frequency changes in spectral measures to prevent or alleviate the detrimental effects of aging on cognition. A possible mechanism behind this reorganization might be the formation of new modules between areas which were not previously connected. At older ages, the higher number of connections (as seen in the theta band) might help the overall functional integration of the brain areas that allows it to cope with the loss in the structural integrity of the neuronal structures. However, this also leads to loss of functional specialization of the underlying large scale networks, which may also be considered detrimental. Thus, functional integration at the expense of functional segregation may act as

an essential mechanism that drives the reorganization of transient brain networks with age.

The large scale resting-state brain networks have been studied in the context of aging for various measures in many studies. In the face of advancing age, cognitive performance decreases in many modalities and tasks, such as working memory, attention, decision-making, etc. The hugely informative dynamics in the resting brain, which pave the way to understanding how the brain can effectively switch from an ‘idle’ state to an attentive state, are usually studied with fMRI BOLD responses. Although fMRI provides a high spatial resolution and a direct correlation between activation of a brain area and a particular task, the slow hemodynamic response poses a challenge in studying fast perceptual processes, which typically occur on a millisecond timescale. This drawback can be overcome by using EEG or MEG, which provide high temporal resolution with a sampling rate of 1000Hz or more. EEG microstates are quasi-stable topographies that model the power over the scalp and cluster these topographies into unique maps recurring over time. This is similar to the HMM approach of defining transient states; however, MEG data provides superior spatial resolution. Source-reconstructed MEG also allows the data-driven characterization of transient states on the basis of both temporal and spectral dynamics. This type of organization of dynamic activity through transient spatial patterns of coordination can provide flexibility in understanding the adaptation required to allow the brain to respond to the rapidly changing computational demands of cognitive processing. Thus, understanding how the short-lived transient states in the context of healthy aging seemed imperative to gain a perspective of how the brain attempts to retain cognitive power as a person gets older.

Chapter 5

Conclusion

Our study highlights the major differences between the spatial, temporal and spectral characteristics of the large scale transient brain networks with age. It provides an important insight into their dynamics and adaptability in healthy aging. The temporal scale considered here is much faster than previously established. We could replicate the patterns of global age-related changes found in the brain using fMRI techniques. The superior temporal resolution of MEG-data and the complete data-driven manner of our state characterization enables us to relate the transient, spontaneous brain dynamics to perception and cognition more meaningfully.

A few limitations of this study include a lack of robust validation performed on the accuracy of the model's prediction. The analysis was performed on group-level measures, which might not allow us to understand the idiosyncrasies in each subject's data. Only one minute of the resting state MEG data was used in this study due to computational power constraints. Including more time points can reveal more unique spatiotemporal activation patterns and might correlate better with known resting-state networks.

Future Directions

An immediate extension of our study could be to increase the number of participants and the number of data points to let the model learn the variability in the data better. A lifespan analysis considering subject level differences rather than group-level differences

can show us a more direct relationship between the measures included in the study with age. Regression analysis could show the exact dependence of the temporal and spectral measures with age. Moreover, the data can be divided into training, testing, and validation sets to ensure high model accuracy. Finally, the analysis could directly be used to study task-related transient brain dynamics to determine how task performance relates to these measures.

References

- [1] D. L. Murman. “The impact of age on cognition”. In: *Seminars in hearing*. Vol. 36. 03. Thieme Medical Publishers. 2015, pp. 111–121.
- [2] C. N. Harada, M. C. N. Love, and K. L. Triebel. “Normal cognitive aging”. In: *Clinics in geriatric medicine* 29.4 (2013), pp. 737–752.
- [3] T. A. Salthouse. “Selective review of cognitive aging”. In: *Journal of the International neuropsychological Society* 16.5 (2010), pp. 754–760.
- [4] R. Levy et al. “Aging-associated cognitive decline”. In: *International Psychogeriatrics* 6.1 (1994), pp. 63–68.
- [5] O. Y. Chén, H. Cao, J. M. Reinen, T. Qian, J. Gou, H. Phan, M. De Vos, and T. D. Cannon. “Resting-state brain information flow predicts cognitive flexibility in humans”. In: *Scientific reports* 9.1 (2019), pp. 1–16.
- [6] E. Varangis, C. G. Habeck, Q. R. Razlighi, and Y. Stern. “The effect of aging on resting state connectivity of predefined networks in the brain”. In: *Frontiers in aging neuroscience* (2019), p. 234.
- [7] J. S. Allen, J. Bruss, C. K. Brown, and H. Damasio. “Normal neuroanatomical variation due to age: the major lobes and a parcellation of the temporal region”. In: *Neurobiology of aging* 26.9 (2005), pp. 1245–1260.
- [8] R. Tibon, K. A. Tsvetanov, D. Price, D. Nesbitt, C. Cam, and R. Henson. “Transient neural network dynamics in cognitive ageing”. In: *Neurobiology of aging* 105 (2021), pp. 217–228.
- [9] S. Taulu and J. Simola. “Spatiotemporal signal space separation method for rejecting nearby interference in MEG measurements”. In: *Physics in Medicine & Biology* 51.7 (2006), p. 1759.

- [10] K. A. Tsvetanov, R. N. Henson, L. K. Tyler, S. W. Davis, M. A. Shafto, J. R. Taylor, N. Williams, and J. B. Rowe. “The effect of ageing on fMRI: Correction for the confounding effects of vascular reactivity evaluated by joint fMRI and MEG in 335 adults”. In: *Human brain mapping* 36.6 (2015), pp. 2248–2269.
- [11] A. F. Fotenos, A. Snyder, L. Girton, J. Morris, and R. Buckner. “Normative estimates of cross-sectional and longitudinal brain volume decline in aging and AD”. In: *Neurology* 64.6 (2005), pp. 1032–1039.
- [12] P. Pieperhoff, L. Hömke, F. Schneider, U. Habel, N. J. Shah, K. Zilles, and K. Amunts. “Deformation field morphometry reveals age-related structural differences between the brains of adults up to 51 years”. In: *Journal of Neuroscience* 28.4 (2008), pp. 828–842.
- [13] F. Kruggel. “MRI-based volumetry of head compartments: normative values of healthy adults”. In: *Neuroimage* 30.1 (2006), pp. 1–11.
- [14] A. Pfefferbaum and E. V. Sullivan. “Increased brain white matter diffusivity in normal adult aging: relationship to anisotropy and partial voluming”. In: *Magnetic Resonance in Medicine: An Official Journal of the International Society for Magnetic Resonance in Medicine* 49.5 (2003), pp. 953–961.
- [15] A. Pfefferbaum, E. V. Sullivan, M. Hedehus, K. O. Lim, E. Adalsteinsson, and M. Moseley. “Age-related decline in brain white matter anisotropy measured with spatially corrected echo-planar diffusion tensor imaging”. In: *Magnetic Resonance in Medicine: An Official Journal of the International Society for Magnetic Resonance in Medicine* 44.2 (2000), pp. 259–268.
- [16] V. A. Magnotta, N. C. Andreasen, S. K. Schultz, G. Harris, T. Cizadlo, D. Heckel, P. Nopoulos, and M. Flaum. “Quantitative in vivo measurement of gyrification in the human brain: changes associated with aging”. In: *Cerebral Cortex* 9.2 (1999), pp. 151–160.
- [17] D. H. Salat, R. L. Buckner, A. Z. Snyder, D. N. Greve, R. S. Desikan, E. Busa, J. C. Morris, A. M. Dale, and B. Fischl. “Thinning of the cerebral cortex in aging”. In: *Cerebral cortex* 14.7 (2004), pp. 721–730.
- [18] N. Erixon-Lindroth, L. Farde, T.-B. R. Wahlin, J. Sovago, C. Halldin, and L. Bäckman. “The role of the striatal dopamine transporter in cognitive aging”. In: *Psychiatry Research: Neuroimaging* 138.1 (2005), pp. 1–12.

- [19] N. D. Volkow, J. Logan, J. S. Fowler, G.-J. Wang, R. C. Gur, C. Wong, C. Felder, S. J. Gatley, Y.-S. Ding, R. Hitzemann, et al. “Association between age-related decline in brain dopamine activity and impairment in frontal and cingulate metabolism”. In: *American Journal of Psychiatry* 157.1 (2000), pp. 75–80.
- [20] Y. I. Sheline, M. A. Mintun, S. M. Moerlein, and A. Z. Snyder. “Greater loss of 5-HT_{2A} receptors in midlife than in late life”. In: *American Journal of Psychiatry* 159.3 (2002), pp. 430–435.
- [21] Y. Zhang, Y. Zhang, P. Cai, H. Luo, and F. Fang. “The causal role of α -oscillations in feature binding”. In: *Proceedings of the National Academy of Sciences* 116.34 (2019), pp. 17023–17028.
- [22] J. J. Foxe and A. C. Snyder. “The role of alpha-band brain oscillations as a sensory suppression mechanism during selective attention”. In: *Frontiers in psychology* 2 (2011), p. 154.
- [23] G. Rohenkohl and A. C. Nobre. “Alpha oscillations related to anticipatory attention follow temporal expectations”. In: *Journal of Neuroscience* 31.40 (2011), pp. 14076–14084.
- [24] K. Thuwal, A. Banerjee, and D. Roy. “Aperiodic and periodic components of ongoing oscillatory brain dynamics link distinct functional aspects of cognition across adult lifespan”. In: *Eneuro* 8.5 (2021).
- [25] B. Sahoo, A. Pathak, G. Deco, A. Banerjee, and D. Roy. “Lifespan associated global patterns of coherent neural communication”. In: *Neuroimage* 216 (2020), p. 116824.
- [26] B. Scally, M. R. Burke, D. Bunce, and J.-F. Delvenne. “Resting-state EEG power and connectivity are associated with alpha peak frequency slowing in healthy aging”. In: *Neurobiology of aging* 71 (2018), pp. 149–155.
- [27] A. Dickinson, C. DiStefano, D. Senturk, and S. S. Jeste. “Peak alpha frequency is a neural marker of cognitive function across the autism spectrum”. In: *European Journal of Neuroscience* 47.6 (2018), pp. 643–651.
- [28] S. Finnigan and I. H. Robertson. “Resting EEG theta power correlates with cognitive performance in healthy older adults”. In: *Psychophysiology* 48.8 (2011), pp. 1083–1087.

- [29] D. J. Mitchell, N. McNaughton, D. Flanagan, and I. J. Kirk. “Frontal-midline theta from the perspective of hippocampal “theta””. In: *Progress in neurobiology* 86.3 (2008), pp. 156–185.
- [30] E. Heinrichs-Graham and T. W. Wilson. “Coding complexity in the human motor circuit”. In: *Human Brain Mapping* 36.12 (2015), pp. 5155–5167.
- [31] E. Heinrichs-Graham, T. J. McDermott, M. S. Mills, A. I. Wiesman, Y.-P. Wang, J. M. Stephen, V. D. Calhoun, and T. W. Wilson. “The lifespan trajectory of neural oscillatory activity in the motor system”. In: *Developmental cognitive neuroscience* 30 (2018), pp. 159–168.
- [32] H. E. Rossiter, E. M. Davis, E. V. Clark, M.-H. Boudrias, and N. S. Ward. “Beta oscillations reflect changes in motor cortex inhibition in healthy ageing”. In: *Neuroimage* 91 (2014), pp. 360–365.
- [33] M. O’Sullivan, D. K. Jones, P. Summers, R. Morris, S. Williams, and H. Markus. “Evidence for cortical “disconnection” as a mechanism of age-related cognitive decline”. In: *Neurology* 57.4 (2001), pp. 632–638.
- [34] J. S. Damoiseaux, C. Beckmann, E. S. Arigita, F. Barkhof, P. Scheltens, C. Stam, S. Smith, and S. Rombouts. “Reduced resting-state brain activity in the “default network” in normal aging”. In: *Cerebral cortex* 18.8 (2008), pp. 1856–1864.
- [35] R. Sala-Llonch, D. Bartrés-Faz, and C. Junqué. “Reorganization of brain networks in aging: a review of functional connectivity studies”. In: *Frontiers in psychology* 6 (2015), p. 663.
- [36] J. R. Andrews-Hanna, A. Z. Snyder, J. L. Vincent, C. Lustig, D. Head, M. E. Raichle, and R. L. Buckner. “Disruption of large-scale brain systems in advanced aging”. In: *Neuron* 56.5 (2007), pp. 924–935.
- [37] N. Filippini, L. Nickerson, C. F. Beckmann, K. P. Ebmeier, G. B. Frisoni, P. M. Matthews, S. M. Smith, and C. E. Mackay. “Age-related adaptations of brain function during a memory task are also present at rest”. In: *Neuroimage* 59.4 (2012), pp. 3821–3828.
- [38] A. M. Mowinckel, T. Espeseth, and L. T. Westlye. “Network-specific effects of age and in-scanner subject motion: a resting-state fMRI study of 238 healthy adults”. In: *Neuroimage* 63.3 (2012), pp. 1364–1373.

- [39] E. A. Allen, E. B. Erhardt, E. Damaraju, W. Gruner, J. M. Segall, R. F. Silva, M. Havlicek, S. Rachakonda, J. Fries, R. Kalyanam, et al. “A baseline for the multivariate comparison of resting-state networks”. In: *Frontiers in systems neuroscience* 5 (2011), p. 2.
- [40] D. Tomasi and N. D. Volkow. “Aging and functional brain networks”. In: *Molecular psychiatry* 17.5 (2012), pp. 549–558.
- [41] K. Onoda, M. Ishihara, and S. Yamaguchi. “Decreased functional connectivity by aging is associated with cognitive decline”. In: *Journal of cognitive neuroscience* 24.11 (2012), pp. 2186–2198.
- [42] A. M. Fjell, M. H. Sneve, H. Grydeland, A. B. Storsve, and K. B. Walhovd. “The disconnected brain and executive function decline in aging”. In: *Cerebral cortex* 27.3 (2017), pp. 2303–2317.
- [43] B. B. Biswal and J. L. Ulmer. “Blind source separation of multiple signal sources of fMRI data sets using independent component analysis”. In: *Journal of computer assisted tomography* 23.2 (1999), pp. 265–271.
- [44] A. Abou Elseoud, H. Littow, J. Remes, T. Starck, J. Nikkinen, J. Nissilä, O. Tervonen, M. Timonen, and V. J. Kiviniemi. “Group-ICA model order highlights patterns of functional brain connectivity”. In: *Frontiers in systems neuroscience* 5 (2011), p. 37.
- [45] C. M. Michel and T. Koenig. “EEG microstates as a tool for studying the temporal dynamics of whole-brain neuronal networks: a review”. In: *Neuroimage* 180 (2018), pp. 577–593.
- [46] N. K. Logothetis. “What we can do and what we cannot do with fMRI”. In: *Nature* 453.7197 (2008), pp. 869–878.
- [47] M. J. Brookes, G. C. O’Neill, E. L. Hall, M. W. Woolrich, A. Baker, S. P. Corner, S. E. Robson, P. G. Morris, and G. R. Barnes. “Measuring temporal, spectral and spatial changes in electrophysiological brain network connectivity”. In: *Neuroimage* 91 (2014), pp. 282–299.
- [48] C. Chang, Z. Liu, M. C. Chen, X. Liu, and J. H. Duyn. “EEG correlates of time-varying BOLD functional connectivity”. In: *Neuroimage* 72 (2013), pp. 227–236.

- [49] F. De Pasquale, S. Della Penna, A. Z. Snyder, C. Lewis, D. Mantini, L. Marzetti, P. Belardinelli, L. Ciancetta, V. Pizzella, G. L. Romani, et al. “Temporal dynamics of spontaneous MEG activity in brain networks”. In: *Proceedings of the National Academy of Sciences* 107.13 (2010), pp. 6040–6045.
- [50] A. J. Quinn, D. Vidaurre, R. Abeysuriya, R. Becker, A. C. Nobre, and M. W. Woolrich. “Task-evoked dynamic network analysis through hidden markov modeling”. In: *Frontiers in neuroscience* 12 (2018), p. 603.
- [51] A. P. Baker, M. J. Brookes, I. A. Rezek, S. M. Smith, T. Behrens, P. J. P. Smith, and M. Woolrich. “Fast transient networks in spontaneous human brain activity”. In: *elife* 3 (2014), e01867.
- [52] D. Vidaurre, A. J. Quinn, A. P. Baker, D. Dupret, A. Tejero-Cantero, and M. W. Woolrich. “Spectrally resolved fast transient brain states in electrophysiological data”. In: *Neuroimage* 126 (2016), pp. 81–95.
- [53] D. Vidaurre, L. T. Hunt, A. J. Quinn, B. A. Hunt, M. J. Brookes, A. C. Nobre, and M. W. Woolrich. “Spontaneous cortical activity transiently organises into frequency specific phase-coupling networks”. In: *Nature communications* 9.1 (2018), pp. 1–13.
- [54] D. Vidaurre, S. M. Smith, and M. W. Woolrich. “Brain network dynamics are hierarchically organized in time”. In: *Proceedings of the National Academy of Sciences* 114.48 (2017), pp. 12827–12832.
- [55] J. R. Taylor, N. Williams, R. Cusack, T. Auer, M. A. Shafto, M. Dixon, L. K. Tyler, R. N. Henson, et al. “The Cambridge Centre for Ageing and Neuroscience (Cam-CAN) data repository: Structural and functional MRI, MEG, and cognitive data from a cross-sectional adult lifespan sample”. In: *Neuroimage* 144 (2017), pp. 262–269.
- [56] M. A. Shafto, L. K. Tyler, M. Dixon, J. R. Taylor, J. B. Rowe, R. Cusack, A. J. Calder, W. D. Marslen-Wilson, J. Duncan, T. Dalgleish, et al. “The Cambridge Centre for Ageing and Neuroscience (Cam-CAN) study protocol: a cross-sectional, lifespan, multidisciplinary examination of healthy cognitive ageing”. In: *BMC neurology* 14.1 (2014), pp. 1–25.
- [57] C. J. Holmes, R. Hoge, L. Collins, R. Woods, A. W. Toga, and A. C. Evans. “Enhancement of MR images using registration for signal averaging”. In: *Journal of computer assisted tomography* 22.2 (1998), pp. 324–333.

- [58] R. S. Desikan, F. Ségonne, B. Fischl, B. T. Quinn, B. C. Dickerson, D. Blacker, R. L. Buckner, A. M. Dale, R. P. Maguire, B. T. Hyman, et al. “An automated labeling system for subdividing the human cerebral cortex on MRI scans into gyral based regions of interest”. In: *Neuroimage* 31.3 (2006), pp. 968–980.
- [59] G. L. Colclough, M. J. Brookes, S. M. Smith, and M. W. Woolrich. “A symmetric multivariate leakage correction for MEG connectomes”. In: *Neuroimage* 117 (2015), pp. 439–448.
- [60] C. J. Stam, G. Nolte, and A. Daffertshofer. “Phase lag index: assessment of functional connectivity from multi channel EEG and MEG with diminished bias from common sources”. In: *Human brain mapping* 28.11 (2007), pp. 1178–1193.
- [61] S. Ganesan, J. Lv, and A. Zalesky. “Multi-timepoint pattern analysis: Influence of personality and behavior on decoding context-dependent brain connectivity dynamics”. In: *Human brain mapping* 43.4 (2022), pp. 1403–1418.
- [62] A. Xifra-Porxas, G. Niso, S. Larivière, M. Kassinopoulos, S. Baillet, G. D. Mitsis, and M.-H. Boudrias. “Older adults exhibit a more pronounced modulation of beta oscillations when performing sustained and dynamic handgrips”. In: *Neuroimage* 201 (2019), p. 116037.
- [63] T. T. Tran, C. E. Rolle, A. Gazzaley, and B. Voytek. “Linked sources of neural noise contribute to age-related cognitive decline”. In: *Journal of cognitive neuroscience* 32.9 (2020), pp. 1813–1822.

Appendix

Table 5.1: Pairwise comparison of cluster based activation values between the age groups. Multiple comparison was performed using Post Hoc Tuley's test for pairwise T-test and controlled for family wise error rate. The asterisk (*) denotes that the differences between the means of the two groups are significant in the 95% interval of confidence. NS denotes the difference between means are not significant.

Age group	Age group	p value	Sig.
Young	Early Middle	0.97	NS
	Late Middle	1.26e-26	*
	Old	0.99	NS
Early middle	Late Middle	2.53e-27	*
	Old	0.99	NS
Late middle	Old	3.98e-27	*

Table 5.2: Pairwise comparison of whole brain activation values between all states. Multiple comparison was performed using Post Hoc Tukey's test for pairwise T-test and controlled for family wise error rate. The asterisk (*) denotes that the differences between the means of the two groups are significant in the 95% interval of confidence. NS denotes the difference between means are not significant. A p -value of zero indicates that the first four digits after the decimal point are zeros.

	State Number	State Number	p value	Sig.
1	2		0.01	*
	3		0	*
	4		0	*
	5		0	*
	6		0	*
	7		1.11e-14	*
	8		0	*
		3	0	*
2	4		0	*
	5		0	*
	6		0	*
	7		0	*
	8		0	*
		3	0	*
	4		0	*
	5		0	*
3	6		0.14	
	7		0.99	
	8		0.11	
		6	0.36	
		7	0	*
		8	0	
		3	0.19	
	4		0.99	
4	5		3.82e-5	*
	6		0	*
	7			
	8			
		6	0.15	
		7	0.27	
		8	0	*
		3		
5	4			
	5			
	6			
	7			
	8			
		4		
		5		
		6		
6	7			
	8			
		4		
		5		
		6		
		7		
		8		
		3		
7	4			
	5			
	6			
	7			
	8			
		4		
		5		
		6		

Table 5.3: Comparisons between transition probabilities from one state to another. An asterisk denotes statistical significance at alpha = 0.05, and NS denotes that the difference between group means are not significant at the given confidence interval.

	State Number	State Number	<i>p</i> value	Sig.
1	2		0.97	NS
	3		0.12	NS
	4		0.96	NS
	5		0.92	NS
	6		0	*
	7		3.00e-3	*
	8		0.91	NS
		3	0.005	*
2	4		0.99	NS
	5		0.99	NS
	6		1.39e-18	*
	7		0.09	NS
	8		0.32	NS
		4	0.004	*
3	5		0.002	*
	6		0	*
	7		2.10e-9	*
	8		0.83	NS
		5	0.99	NS
4	6		2.12e-18	*
	7		1.07e-1	*
	8		0.29	NS
		6	1.39e-17	*
5	7		0.16	NS
	8		0.2	NS
		7	1.99e-8	*
6	8		0	*
		7	1.26e-5	*
7		8		

Table 5.4: Pairwise comparison of whole brain phase lag index values of all age groups in the theta band frequency range. Multiple comparison was performed using Post Hoc Tukey's test for pairwise T-test and controlled for family wise error rate. The asterisk (*) denotes that the differences between the means of the two groups are significant in the 95% interval of confidence. NS denotes the difference between means are not significant.

Age group	Age group	p value	Sig.
Young	Early Middle	9.85e-5	*
	Late Middle	3.05e-8	*
	Old	0	*
Early middle	Late Middle	0.41	NS
	Old	9.35e-18	*
Late middle	Old	5.14e-12	*

Table 5.5: Pairwise comparison of whole brain phase lag index values of all age groups in the alpha band frequency range. Multiple comparison was performed using Post Hoc Tukey's test for pairwise T-test and controlled for family wise error rate. The asterisk (*) denotes that the differences between the means of the two groups are significant in the 95% interval of confidence. NS denotes the difference between means are not significant.

Age group	Age group	p value	Sig.
Young	Early Middle	0.95	NS
	Late Middle	0.68	NS
	Old	3.89e-8	*
Early middle	Late Middle	0.93	NS
	Old	1.66e-9	*
Late middle	Old	2.72e-11	*

(a) Pairwise comparison of cluster based coherence values between age groups

Age group	Age group	p value	Sig.
Young	Early Middle	9.31e-14	*
	Late Middle	0	*
	Old	1.18e-5	*
Early middle	Late Middle	5.16e-4	*
	Old	0.02	*
	Late middle	Old	5.43e-11 *

(b) Pairwise comparison of cluster based coherence values between age groups

Age group	Age group	p value	Sig.
Young	Early Middle	0	*
	Late Middle	0	*
	Old	0.99	NS
Early middle	Late Middle	0.28	NS
	Old	0	*
	Late middle	Old	0 *

Table 5.6: Cluster based coherence values and their comparison between age groups. The significant differences are denoted by an asterisk. Non-significant differences are marked as NS.

(a) Pairwise comparison of cluster based PLI values between age groups

Age group	Age group	<i>p</i> value	Sig.
Young	Early Middle	0.14	NS
	Late Middle	0.99	NS
	Old	0.31	NS
Early middle	Late Middle	0.19	NS
	Old	0.98	NS
	Late middle	0.39	NS

(b) Pairwise comparison of cluster based PLI values between age groups

Age group	Age group	<i>p</i> value	Sig.
Young	Early Middle	1.00	NS
	Late Middle	0.85	NS
	Old	0.97	NS
Early middle	Late Middle	0.84	NS
	Old	0.96	NS
	Late middle	0.99	NS

Table 5.7: Cluster based PLI values and their comparison between age groups. Tables 5.7a and 5.7b shows no significant changes across age groups (NS = non-significant) in both of the frequency ranges.